

Functional Properties of Neurons in Macaque Area V3

KARL R. GEGENFURTNER,¹ DANIEL C. KIPER,² AND JONATHAN B. LEVITT³

¹Max-Planck-Institut für Biologische Kybernetik, 72076 Tübingen, Germany; ²Institut d'Anatomie, Faculté de Médecine, Université de Lausanne, 1005 Lausanne, Switzerland; and ³Department of Visual Science, Institute of Ophthalmology, University College London, London EC1V 9EL, United Kingdom

Gegenfurtner, Karl R., Daniel C. Kiper, and Jonathan B. Levitt. Functional properties of neurons in macaque area V3. *J. Neurophysiol.* 77: 1906–1923, 1997. We investigated the functional properties of neurons in extrastriate area V3. V3 receives inputs from both magno- and parvocellular pathways and has prominent projections to both the middle temporal area (area MT) and V4. It may therefore represent an important site for integration and transformation of visual signals. We recorded the activity of single units representing the central 10° in anesthetized, paralyzed macaque monkeys. We measured each cell's spatial, temporal, chromatic, and motion properties with the use of a variety of stimuli. Results were compared with measurements made in V2 neurons at similar eccentricities. Similar to area V2, most of the neurons in our sample (80%) were orientation selective, and the distribution of orientation bandwidths was similar to that found in V2. Neurons in V3 preferred lower spatial and higher temporal frequencies than V2 neurons. Contrast thresholds of V3 neurons were extremely low. Achromatic contrast sensitivity was much higher than in V2, and similar to that found in MT. About 40% of all neurons showed strong directional selectivity. We did not find strongly directional cells in layer 4 of V3, the layer in which the bulk of V1 and V2 inputs terminate. This property seems to be developed within area V3. An analysis of the responses of directionally selective cells to plaid patterns showed that in area V3, as in MT and unlike in V1 and V2, there exist cells sensitive to the motion of the plaid pattern rather than to that of the components. The exact proportion of cells classified as being selective to color depended to a large degree on the experiment and on the criteria used for classification. With the use of the same conditions as in a previous study of V2 cells, we found as many (54%) color-selective cells as in V2 (50%). Furthermore, the responses of V3 cells to colored sinusoidal gratings were well described by a linear combination of cone inputs. The two subpopulations of cells responsive to color and to motion overlapped to a large extent, and we found a significant proportion of cells that gave reliable and directional responses to drifting isoluminant gratings. Our results show that there is a significant interaction between color and motion processing in area V3, and that V3 cells exhibit the more complex motion properties typically observed at later stages of visual processing.

INTRODUCTION

Little is known about the functional properties of cells in V3. This might be partially due to the fact that V3 does not easily fit into a scheme of parallel and independent processing of information in the visual pathway. The division of visual signals into separate pathways for the processing of color, form, motion, and depth has been serving as a guideline for our understanding of the architecture and function of the visual system. One pathway, directed to visual areas of the posterior parietal lobe, is thought to be important for the perception of visual motion, visuospatial analyses, oculomotor behavior, and

direction of visual attention. Another pathway, directed to visual areas of the inferior temporal cortex, seems important for detailed analysis of the form and color of objects. Such differences have led to the description of these two pathways as “what” versus “where” pathways (Ungerleider and Mishkin 1982), or for “motion” versus “color and form” (Livingstone and Hubel 1988; Zeki 1978c).

However, despite much evidence for functional segregation in the visual cortex, it is now also becoming clear that this segregation is not absolute. For example, area V2, which provides a major excitatory drive to both V4 and the middle temporal area (area MT), has been shown to contain prominent intrinsic anatomic connections between different cytochrome oxidase (CO) compartments (Levitt et al. 1994b), and this anatomic cross talk is reflected in the homogeneity of a number of physiological properties across V2 (Gegenfurtner et al. 1996; Levitt et al. 1994a; Peterhans and von der Heydt 1993). Furthermore, there do exist anatomic connections between cortical areas purported to perform different analyses, e.g., V4 and MT (see Felleman and Van Essen 1991).

In that light, the role of cortical area V3 becomes particularly interesting because this area is known to have prominent connections with both cortical functional streams, in particular with areas V4 and MT. It may therefore represent an important site for the coordinated activity of both pathways, as well as for the integration of different stimulus attributes for visual perception.

In many respects, V3 resembles other areas in the parietal motion analysis pathway. It receives an input from V1 (Burkhalter et al. 1986; Felleman and Van Essen 1987; Van Essen et al. 1986; Zeki 1978a,b), mainly from layer 4B, which is necessary for its visual responsiveness (Girard et al. 1991). Furthermore, V3 shows intense immunoreactivity for the Cat-301 antigen (DeYoe et al. 1990), like V1 layer 4B and area MT and unlike inferotemporal visual areas. V3 also contains many directionally selective cells (Felleman and Van Essen 1987), more in fact than any other area except MT (Albright 1984; Dubner and Zeki 1971). Although initial reports suggested color selectivity was rare or absent in V3 (Baizer 1982; Zeki 1978b,c), more recent studies have reported a higher proportion of color-selective and endstopped cells (Burkhalter et al. 1986; Felleman and Van Essen 1987). Further evidence for V3 functions other than motion analysis, for example higher-order form analysis, was seen in multi-peaked orientation or direction tuning of V3 neurons (Felleman and Van Essen 1987). The presence of these different selectivities for stimulus attributes is consistent with the pattern of V3's cortical connections to both areas V4 and MT.

Although we have some knowledge of the topographic representation of the visual field in this area (Gattass et al. 1988; Van Essen and Zeki 1978; Zeki 1978b), and of some basic receptive field properties (Baizer 1982; Felleman and Van Essen 1987; Zeki 1978b,c), little is known about the functional properties of cells in V3. We therefore examined more closely the color and spatial properties of V3 neurons. Unlike V1 or V2, where there is evidence for compartmentalization of function, no suborganization has been found yet in V3. We explored the possibility that information about different stimulus attributes could be combined in V3. Whenever possible, we compared the characteristics of the neuronal responses in V3 with those in area V2.

METHODS

Preparation and maintenance

These experiments were performed on 12 adult macaque monkeys (*Macaca mulatta* or *Macaca fascicularis*). All procedures conformed to National Institutes of Health guidelines. Animals were initially premedicated with atropine (0.25 mg) and acepromazine maleate (PromAce: 0.05 mg/kg). Surgery was performed after induction of anesthesia with intramuscular injections of ketamine (Vetalar: 10–30 mg/kg), and, after cannulation of the saphenous veins, under intravenous anesthesia with Sufentanil citrate as described below.

After the trachea was cannulated, the animal's head was fixed in a stereotaxic frame. A small craniotomy was made over the lunate sulcus. After a small slit was made in the dura, a tungsten-in-glass microelectrode (Merrill and Ainsworth 1972) was positioned ~1–3 mm behind the lip of the sulcus, directed anteriorly to the buried annectant gyrus at an angle of 20° from vertical. Then the hole was covered with warm agar. Action potentials were conventionally amplified and displayed; standard pulses triggered by each impulse were stored by a personal computer (resolution 250 μ s) and were also fed to an audiomonitor.

On completion of surgery, animals were paralyzed to minimize eye movements. Paralysis was maintained with an infusion of vecuronium bromide (Norcuron: 0.1 mg \cdot kg⁻¹ \cdot h⁻¹) in lactated Ringer solution with dextrose (5.4 ml/h). Animals were artificially ventilated with room air or with 49% N₂O-49% O₂-2% CO₂. Peak expired CO₂ was maintained near 4.0% by adjusting the respirator stroke volume or the CO₂ content in the gas mixture. Rectal temperature was kept near 37°C with a thermostatically controlled heating pad. Animals were maintained on a continuous infusion of Sufentanil citrate, the dosage of which was typically 4–8 μ g \cdot kg⁻¹ \cdot h⁻¹, adjusted according to each animal's tolerance to the drug. This was determined before paralysis by testing the animal's reaction to mildly noxious stimuli and making sure that no motor responses could be elicited. After paralysis, electroencephalogram desynchronization and alterations in cardiac rhythm following a noxious stimulus were taken as signals to increase the level of anesthesia. Electrocardiogram, electroencephalogram, and rectal temperature were monitored continuously to ensure the adequacy of anesthesia and the soundness of the animal's physiological condition. Animals also received daily injections of a broad-spectrum antibiotic (Bicillin: 300,000 U) as well as dexamethasone (Decadron: 0.5 mg/kg) to prevent cerebral edema.

The pupils were dilated and accommodation paralyzed with topical atropine. Corneas were protected with gas-permeable contact lenses; supplementary lenses were chosen that maximized the spatial resolution of the first recorded units. Lenses were removed periodically for cleaning and the eyes were rinsed with saline. At the beginning of the experiment, and at regular intervals thereafter,

the foveas were located and plotted with the use of a reversible ophthalmoscope.

Anatomic methods

At the conclusion of the recording session, all animals were killed by a lethal overdose of pentobarbital sodium and perfused through the heart with buffered 4% paraformaldehyde after exsanguination with heparinized saline. Tissue blocks containing the penetrations were allowed to equilibrate in 30% sucrose. Frozen sections were then cut at 40 μ m in the coronal or sagittal planes, and adjacent series of sections were stained for myelin (Gallyas 1979) or cresyl violet.

Track reconstruction and identification of area V3

Sections containing electrode tracks were drawn at low power with the use of a Zeiss Axiophot microscope equipped with a camera lucida. Adjacent sections were aligned precisely with the use of blood vessels and the section outlines as fiducial marks. The laminar locations of the recorded units were assigned on the basis of distance from recorded gray/white matter transitions and from electrolytic lesions made during the recording sessions (electrode tip negative: 2–3 μ A for 3 s). If there were insufficient data to permit assignment to a layer, only designations of "superficial" and "deep" were used for the extremes of the penetration; units whose location could not be specified were omitted from laminar analyses.

Electrode penetrations were directed toward the fundus of the lunate sulcus and the annectant gyrus buried within the lunate sulcus. We used the stereotypical sequence of gray/white matter transitions to help us determine when we had entered V3. Tracks typically started in V1, passed through the underlying white matter and area V2 on the posterior bank of the lunate sulcus, and then went through a silent region as the electrode went through the lunate sulcus, before reentering gray matter in area V3 in which we typically encountered brisk responses that were most often directionally selective. If our penetrations were directed too far anteriorly on the dorsal bank of the lunate sulcus (into area V4), responses were generally weak and inconsistent. However, area V3 cannot be reliably identified on the basis of physiological criteria alone; we therefore relied on postmortem histological criteria. As has been described earlier (Burkhalter et al. 1986; Felleman and Van Essen 1987; Girard et al. 1991; Van Essen et al. 1986), V3 can be identified by its distinctive myeloarchitecture. Figure 1 shows a parasagittal section through the annectant gyrus. Figure 1A is a line drawing of the entire occipital cortex; the region bounded by the solid rectangle is shown in the photomicrograph in B. Arrowheads indicate the approximate boundaries of V3, which can be recognized by its dense myelination in layers 4, 5, and 6. The inner band of Baillarger is thus not separated from the white matter by a clear gap (as in V2 and V3A), and the outer band of Baillarger is faint or absent. We accepted recording sites as being within V3 only if they were within the densely myelinated zone at the crest or posterior bank of the annectant gyrus or on the floor of the lunate sulcus. Although the precise borders of V3 are indistinct in Gallyas-stained material, our recordings avoided these border zones. The anterior border of V3 with V3A is known to represent the inferior vertical meridian (Gattass et al. 1988; Van Essen and Zeki 1978; Van Essen et al. 1986; Zeki 1969). Consistent with this, our recording sites always avoided the vertical meridian, thus seeking to ensure that neurons within V3A were not included in our sample. However, because of possible imprecision in plotting the foveae, and the known irregularities in receptive field topography in extrastriate cortex, we always ultimately relied on postmortem histological identification of recording sites to determine whether we had been in V3.

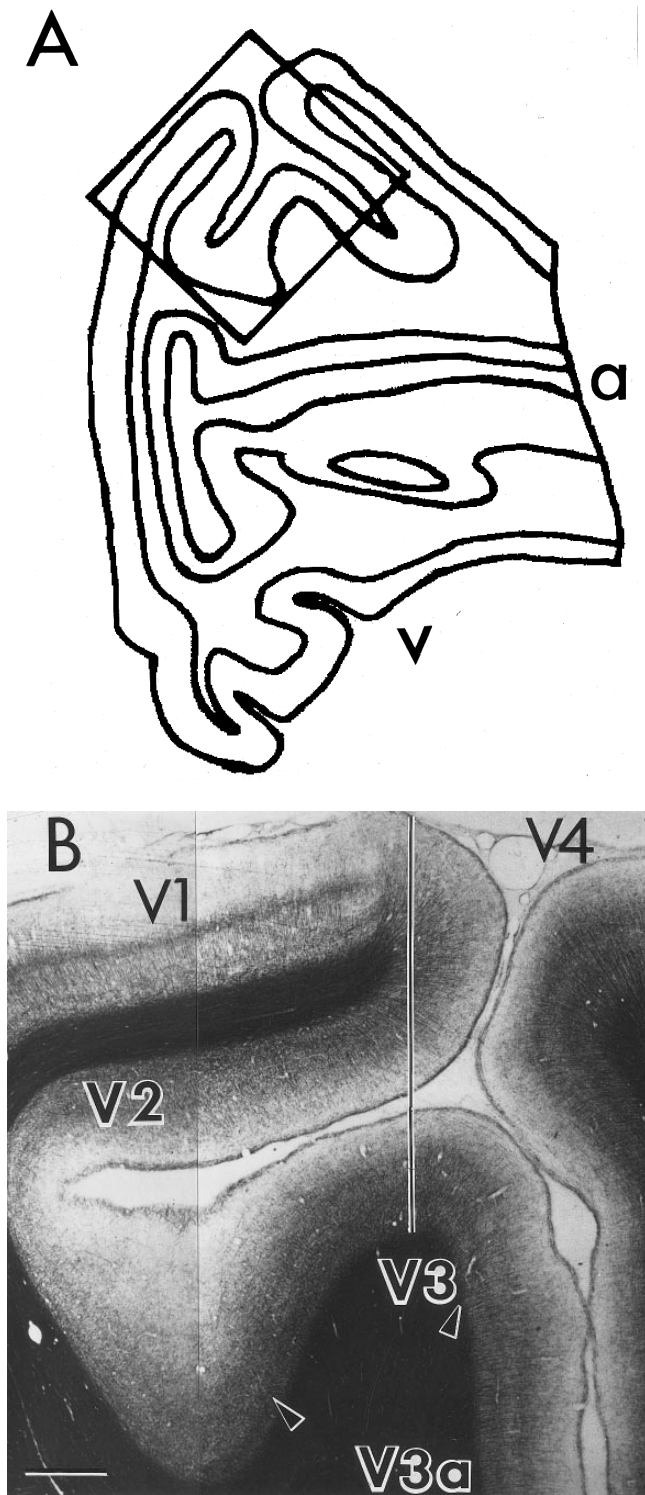


FIG. 1. A: line drawing of a parasagittal section through occipital cortex at the level of the annectant gyrus. Solid rectangle: area shown in the photomicrograph in B. a, anterior; v, ventral. B: photomicrograph of parasagittal section stained for myelin by the method of Gallyas (1979). Arrowheads: uncertainty limits of myeloarchitectonic borders with V2 and V3A. Vertical line: trajectory of electrode penetration. Scale bar: 1 mm.

Characterization of receptive fields

Receptive fields were initially mapped by hand on a tangent screen with the use of black-and-white or colored geometric targets. When a

single neuron's activity was isolated, we established the neuron's dominant eye and occluded the other eye for quantitative experiments. Generally there was little difference between left and right eye. Very few neurons responded to binocular stimulation only. We first mapped the location and size of the neuron's minimum response field (Barlow et al. 1967), and then determined selectivity for the orientation, direction of motion, and size (particularly endstopping) of stimuli. After this initial qualitative characterization, we positioned the receptive field on the face of a display cathode ray tube, and quantitative experiments proceeded under control of a personal computer.

Each experiment consisted of several blocks of trials. Within each block, all stimuli were presented for the same amount of time, generally 4 s. There were a few units that showed signs of adaptation; for those we used stimuli of shorter durations. To minimize effects of response variability, stimuli were presented in a random order within each experimental block, and the results of several repeated blocks (typically between 4 and 8) were averaged. We also always measured responses to a uniform grey field of the same mean luminance as our other stimuli to measure the cell's spontaneous firing rate. Responses were compiled into average histograms synchronized to each temporal cycle of the stimulus. These histograms were then Fourier analyzed to calculate the mean firing rate and the response at the fundamental stimulus frequency. For complex cells, which respond with an unmodulated elevation in discharge rate, we used the mean firing rate response (mean firing rate minus spontaneous activity) as the response measure; for simple cells we used the fundamental stimulus frequency response.

Visual stimulation

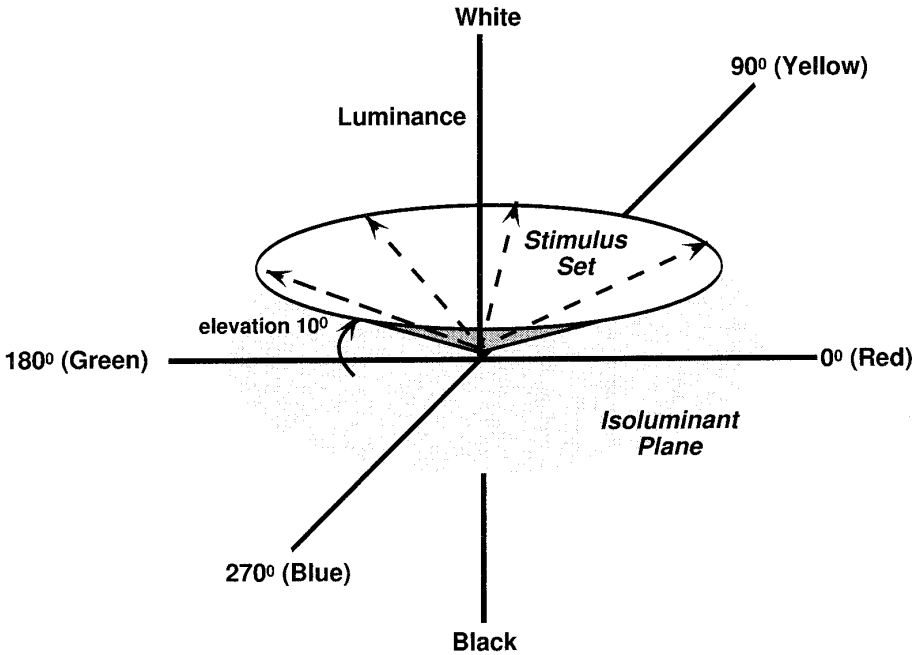
Stimuli were displayed on a BARCO ICD 451B color television monitor driven by an AT Truevision Vista Graphics board. At a viewing distance of 114 cm, the screen subtended $13^\circ \times 13^\circ$ of visual angle. Drifting sinusoidal grating stimuli were modulated in color around an average white point with C.I.E. x, y coordinates of (0.31, 0.32) with an average luminance of 37.5 cd/m^2 . Except for contrast response measurements, contrast of achromatic stimuli was held fixed at 75%. The color stimuli we used are illustrated in detail in Fig. 2. Color modulations were defined along the three cardinal directions of the color space introduced by Krauskopf et al. (1982). At the origin is a neutral white. Along the "L-M" axis, the excitation of the long (L) and middle (M) wavelength-sensitive cones covaries so as to keep their sum constant. Along the "S - (L + M)" axis, only the excitation of the short-wavelength-sensitive (S) cones varies. Along the "luminance" axis, the excitation of all three cones varies in proportion to their excitation at the white point. We will frequently use polar coordinates to describe stimuli in this space. With these a stimulus is defined by its azimuth, which is the angle made by the projection of the stimulus on the isoluminant plane with the L-M axis, and its angular elevation above the isoluminant plane. We used two types of stimuli to measure the color properties of cells. 1) Sinusoidal gratings of varying azimuth with a fixed luminance component of 10% contrast. The inverted cone in Fig. 2A shows these stimuli. 2) Periodic square wave gratings consisting of colored bars on a black background. The colored bars were all of equal luminance (37.5 cd/m^2) and were distributed in color space along an ellipse centered at the white point. Figure 2B shows the distribution of colors in the C.I.E. x, y chromaticity diagram. The two isoluminant cardinal directions are indicated by the dashed lines in Fig. 2B. The magnitude of all color modulations was chosen to be the 75% of the maximum around the given white point. For stimuli in the red and green directions this resulted in a 5 and 9% contrast in the L and M cones, respectively. For stimuli in the blue and yellow directions only S cones were differentially excited, resulting in a 60% S cone contrast.

RESULTS

Description of basic experiments

We recorded from 171 single neurons in area V3 of 12 macaque monkeys. Most of our sample comes from experi-

A



B

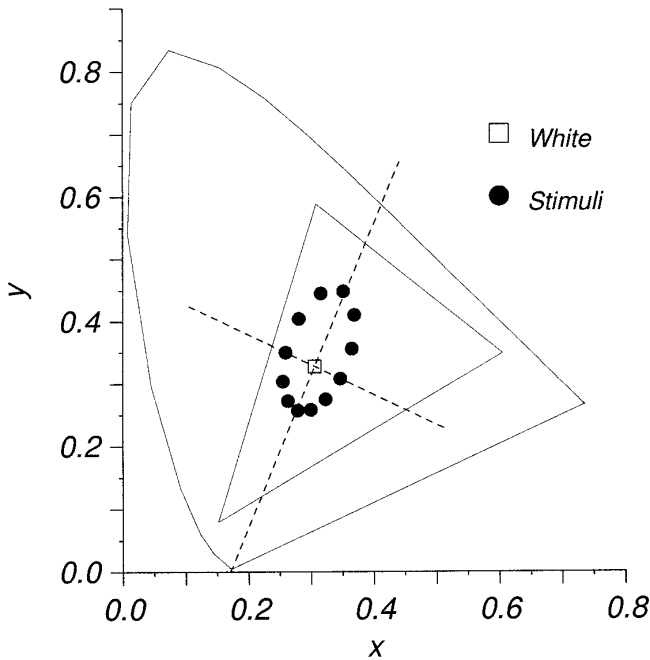


FIG. 2. A: schematic diagram illustrating the color stimuli used in the color experiments. The color space we used has been described in detail elsewhere (Derrington et al. 1984; Krauskopf et al. 1982). At the origin is a neutral white. Along the "L-M" axis, the excitation of the long (L) and middle (M) wavelength-sensitive cones covaries so as to keep their sum constant. Along the "S - (L + M)" axis, only the excitation of the short-wavelength-sensitive (S) cones varies. Along the "luminance" axis, the excitation of all 3 cones varies in proportion to their excitation at the white point. A stimulus in this space is defined by its azimuth, which is the angle made by its projection on the isoluminant plane with the L-M axis, and its angular elevation above the isoluminant plane. The inverted cone represents the set of stimuli with an elevation of 10° and an azimuth varying between 0 and 360°. The scaling of the three axes in this space is arbitrary; in our experiments the maximum modulation was 100% luminance contrast along the luminance axis, 85% S cone contrast along the S (L + M) axis, and 13% M cone modulation along the L-M axis. B: C.I.E. x,y chromaticity diagram illustrating the same color stimuli. Dashed lines: placement of the axis of the color space described above. Triangle: C.I.E. coordinates of the phosphors of our monitor. Because the mean luminance of our stimuli was higher than the maximum luminance of the red and the blue phosphors, the range of color was even more restricted than the triangle.

ments on five rhesus monkeys, in which our target area was V3. Data from an additional 37 V3 cells come from earlier experiments in seven *M. fascicularis*, aimed at investigating neuronal responses in area V2 (Gegenfurtner et al. 1996), but in which some cells were found to have been located in area V3. Experimental methods were identical in both sets of experiments. Seventy-five percent of the units had receptive fields centered within 5° of the fovea; the remaining receptive fields were within 8°. Minimum response fields, as

determined by receptive field plotting, were typically ~2.5° × 2.5°. For each neuron we measured the tuning and sensitivity to otherwise optimal stimuli of different orientation and direction, spatial frequency, temporal frequency, size, contrast, and color, in that order. Most of the cells (85%) were complex-like and responded with an elevation in discharge. The proportion of simple cells (15%) was lower than the 25% that was found in area V2 (Levitt et al. 1994a).

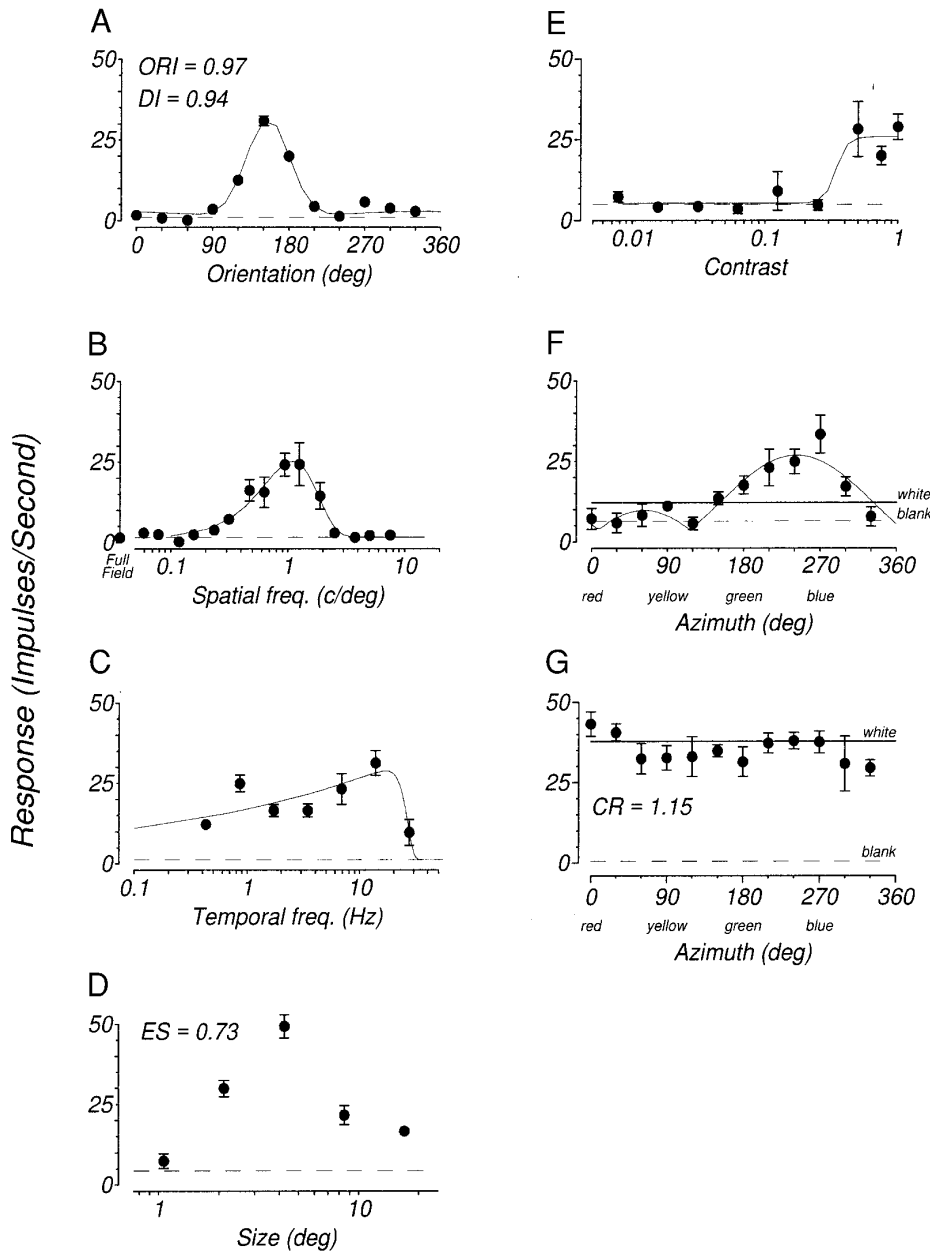


FIG. 3. Description of basic experiments. Responses are from a single V3 cell. In all graphs the Y-axis shows the response in imp/s. Dashed horizontal line: response to a gray uniform field. Thin curve in all graphs (except *D* and *G*): fit of a smooth function. *A*: responses to black-and-white sinusoidal gratings of different orientations. We defined a direction index $DI = 1 - (\text{response in opposite direction} - \text{baseline}) / (\text{response in optimum direction} - \text{baseline})$ and an orientation index $ORI = 1 - (\text{response in orthogonal orientation} - \text{baseline}) / (\text{response in optimum orientation} - \text{baseline})$. This cell was orientation selective and also strongly selective for direction of motion. *B*: responses to sinusoidal grating patches of different spatial frequencies. *C*: responses to sinusoidal grating patches of different temporal frequencies. *D*: responses to sinusoidal grating patches of different sizes. Endstopping index (ES) was defined as $ES = 1 - (\text{response to largest stimulus} - \text{baseline}) / (\text{response to optimum stimulus} - \text{baseline})$. This cell was strongly endstopped. *E*: responses to sinusoidal grating patches of different contrast. *F*: responses to sinusoidal grating patches whose color is modulated around a neutral white point. All stimuli had a fixed luminance contrast of 10%. Azimuth: azimuth of the brighter bars, i.e., red stands for bright red and dark green bars. Solid horizontal line: response to a black-and-white grating of 10% luminance contrast. *G*: responses to bars of different color on a black background. Solid horizontal line: response to a white bar of the same luminance (37.5 cd/m^2) as the colored bars. We defined color responsivity index (CR) as $CR = (\text{best response to colored bar} - \text{baseline}) / (\text{response to white bar} - \text{baseline})$.

Figure 3 shows responses obtained from a single V3 cell and illustrates the basic experiments in the order in which they were run. Figure 3A shows responses to black-and-white sinusoidal gratings moving at different orientations. Gratings were of optimal spatial and temporal frequency and size. This cell responded very briskly to gratings oriented at an angle of $\sim 150^\circ$ (drifting upward and to the right), and did not give any response at the orthogonal orientations or the opposite direction of motion. The dashed horizontal line shows the spontaneous activity level of the cell. SEs of the response are also shown. However, for this cell they were smaller than the symbols in most cases. We fitted a smooth function through the data points (shown by the solid curve) and defined a direction index (DI)

$$DI = 1 - \frac{\text{response in opposite direction} - \text{baseline}}{\text{response in optimum direction} - \text{baseline}}$$

and an orientation index (ORI)

$$ORI = 1 - \frac{\text{response in orthogonal orientation} - \text{baseline}}{\text{response in optimum orientation} - \text{baseline}}$$

Cells with $DI > 0.7$ were classified as directionally selective (40% of our V3 sample); cells with $ORI > 0.7$ were classified as oriented (80%). These criteria require at least a three-fold increase in firing at the optimum (relative to orthogonal orientation or opposite direction of motion) for a cell to be classified as directionally selective or orientation selective. For the cell in Fig. 3A, the values of DI and ORI are both close to 1, indicating that the responses are almost at the level of the baseline for the opposite direction and at the orthogonal orientation.

Figure 3B shows responses to sinusoidal gratings of different spatial frequencies. We fit a smooth function to the

data, defined by a difference of exponentials, to extract parameters for the spatial frequency tuning. This cell showed a response peak at ~ 1 cycle/degree, which is typical for our sample of V3 cells. We defined the high cutoff frequency as the spatial frequency at which the cell's response fell to half the peak response.

Figure 3C shows responses to sinusoidal gratings of different temporal frequencies. We fit the data with a difference of exponentials to extract parameters for the temporal frequency tuning. As is typical in V3, this cell showed a rather broad tuning and responded at all low and medium temporal frequencies, with a peak at ~ 20 Hz. Its high cutoff, the point at which the response fell to half the peak, is at ~ 25 Hz.

Figure 3D shows responses of the same cell to black-and-white sinusoidal gratings of different sizes. In our experiments we restricted our stimuli to square patches, and size refers to the width or height of the square stimulus window. All other parameters were set to optimize the cell's response. Endstopping index (ES) was defined as

$$ES = 1 - \frac{\text{response to largest stimulus} - \text{baseline}}{\text{response to optimum stimulus} - \text{baseline}}$$

Cells with $ES > 0.5$ were classified as being endstopped. This cell was significantly inhibited by large stimuli. Its response to a 10° wide stimulus was $\sim 25\%$ of its response to a 5° wide stimulus ($ES = 0.73$).

Figure 3E shows responses to black-and-white sinusoidal gratings of different contrast. We fitted a Naka-Rushton equation

$$R = b + \frac{C^\gamma}{C^\gamma + C_s^\gamma}$$

to the data, where R is the predicted response, b is the response baseline (which was taken from the data and not estimated), C_s is the semisaturation contrast (contrast at which response equals half of the peak response), and γ is the exponent. We used these parameters to characterize the contrast response of the cell. Furthermore, we computed each cell's sensitivity as the inverse of threshold contrast. Threshold contrast was defined as the contrast level where the cell's response exceeded the baseline response plus $1.96 \times SD$ of the baseline response. Because of this definition, sensitivity could not be calculated for cells without spontaneous discharge. The cell in Fig. 3E showed a very steep contrast response with an exponent > 10 . It reached 50% of its maximum response at 35% contrast. Contrast threshold was at 31.1% contrast. At 3.2, sensitivity for this cell is therefore rather low.

Figure 3F shows the responses of the same cell to sinusoidal gratings that were modulated in different color directions around a central white point. In this experiment the cell responds best to gratings consisting of bright blue and dark yellow bars. All the gratings in this experiment had a luminance contrast of 10% and correspond to the points around the circumference of the cone in Fig. 2A. The small response to a black-and-white grating of that luminance contrast is indicated by the solid horizontal line. The curve through the data points represents the best fit of a model that linearly combines cone inputs (Derrington et al. 1984), used to determine the cell's preferred azimuth and elevation.

Responses to bars of different colors are shown in Fig.

3G. Stimuli in this experiment were square wave gratings made of alternating black and colored bars. Orientation, spatial and temporal frequency, and size were set to the cell's preferred values. The solid horizontal line shows the response to a white bar of the same luminance (37.5 cd/m^2) as the colored bars. We defined color responsivity index (CR) as

$$CR = \frac{\text{best response to colored bar} - \text{baseline}}{\text{response to white bar} - \text{baseline}}$$

Cells with $CR > 1.4$ were classified as color selective. For this cell there was little difference in the responses to the various colored bars. The slight increase in firing rate for a bar of azimuth 0 (red) results in a small color responsivity ($CR = 1.15$). As described below, we use CR as an index of color selectivity mainly to allow a direct comparison with earlier data from area V2.

Orientation selectivity

All V3 cells showed some modulation of the orientation tuning function, but only 20% of cells showed a significant response at the orthogonal orientation. Nondirectional cells (60%) always had a second peak in the direction opposite to the preferred one. We did not observe any cells with more than two peaks within 180° in their orientation tuning function. The median orientation half bandwidth at half height was 27.2° , which is remarkably similar to values found in area V2 (Gegenfurtner et al. 1996: 26.7° ; Levitt et al. 1994a: 29°).

Directional selectivity

A substantial proportion of cells in our sample (56 of 141, 39.7%) was strongly directionally selective ($DI > 0.7$), and 24 further cells (17%) were directionally biased ($DI > 0.5$). This makes a total of 56.7% of cells in V3 with directional selectivity. This is more than in any other visual cortical area except MT, which has $\sim 90\%$ directional selectivity (Albright 1984; Dubner and Zeki 1971). In particular, this percentage is higher than in area V2, where $\sim 20\%$ of all cells are strongly directional, and 32% at least directionally biased (Gegenfurtner et al. 1996; Levitt et al. 1994a; Peterhans and von der Heydt 1993). This percentage is only slightly higher in V2 thick stripes, where $\sim 28\%$ of cells are strongly directional and 37.5% at least directionally biased (Gegenfurtner et al. 1996).

Spatiotemporal tuning

Figure 4 summarizes the spatial and temporal tuning properties of all our V3 cells. For comparison, the median values for a comparable sample of V2 neurons (Gegenfurtner et al. 1996) are also given. Figure 4A shows the distribution of peak spatial frequencies of 134 V3 neurons. The neurons were generally tuned to relatively low spatial frequencies, with a median of 0.4 cycles/degree. Roughly 80% of all cells had their peak spatial frequency at ≤ 1 cycle/degree. The median value of the sample of 121 V2 cells at similar eccentricities, indicated by the open arrow, was 1.24 cycles/degree. This difference was highly significant (Mann-Whitney U test, $P < 0.001$). Similarly, as shown in Fig. 4B, the

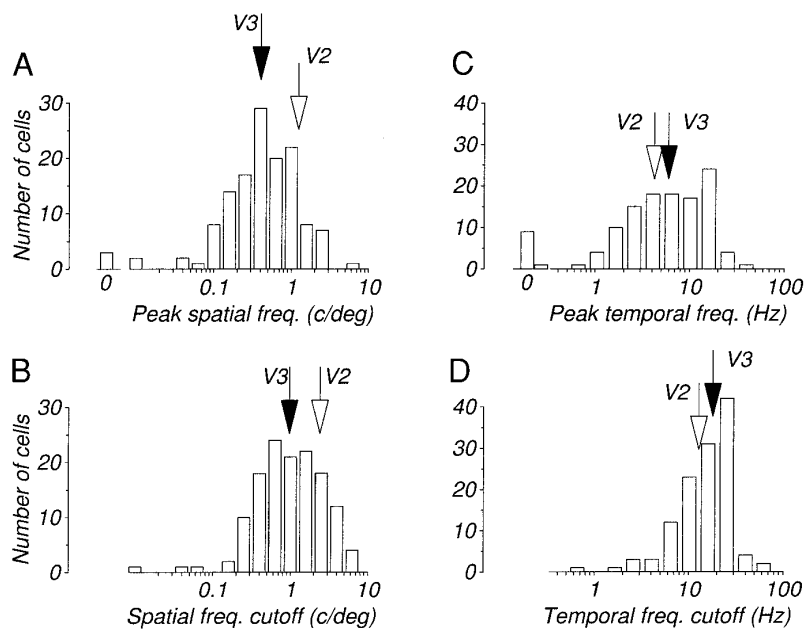


FIG. 4. Spatiotemporal tuning properties of neurons in V3. Filled arrows: median value of V3 cells. Open arrows: median of the corresponding measure of a sample of V2 neurons at similar eccentricities. A: peak spatial frequencies for 134 V3 neurons. B: spatial frequency cutoffs (at half height). C: peak temporal frequencies for 122 V3 neurons. D: temporal frequency cutoffs (at half height).

spatial frequency cutoff at half height is smaller for the V3 cells than it is for the V2 cells. The median cutoff in V3 was 0.97 cycles/degree, compared with 2.4 cycles/degree in the V2 sample. Hardly any of the cells in our sample of V3 cells gave a significant response at >4 cycles/degree.

Peak spatial frequency depends on the size of the receptive field, which in turn depends on eccentricity. Although the range of eccentricities in our V2 and V3 samples were similar, the average eccentricity in V2 was lower by $\sim 1-2^\circ$. We therefore trimmed our V2 sample so that its median eccentricity matched that of the V3 sample. This was done by excluding the cells closest to the fovea. Although the median peak spatial frequency of the reduced V2 sample was indeed lower (0.82 cycles/degree), the difference from the V3 sample was still highly significant (Mann-Whitney U test, $P < 0.001$). The difference in peak spatial frequencies between areas V2 and V3 is therefore not due to differences in the eccentricities of both samples. It reflects a genuine difference in the properties of neurons in these two areas.

Whereas V3 cells are tuned to lower spatial frequencies than V2 cells, they are tuned to higher temporal frequencies, as can be seen in Fig. 4, C and D. In addition, the temporal frequency tuning of V3 neurons is quite broad and typically covers the whole temporal frequency range, as shown in the example in Fig. 3F. The tuning is quite flat over a wide range of temporal frequencies, and therefore the peak is not well defined. Therefore peak temporal frequencies show a large variation and are almost evenly distributed over the whole range. The average temporal frequency bandwidth is 4.4 octaves. Figure 4C shows the distribution of peak temporal frequencies of 122 V3 cells. Thirteen of the cells are low-pass, responding best to stationary or slow stimuli. But even these cells usually responded well at high temporal frequencies. The median peak temporal frequency was at 6 Hz. In comparison, the median peak for a comparable sample of 121 V2 cells was 4.2 Hz. Once again, this difference was statistically significant (Mann-Whitney U test, $P < 0.01$) and remained significant when the two samples were

matched for eccentricity ($P < 0.05$). The high temporal frequency cutoff at half height, shown in Fig. 4D, was also greater for the V3 cells (median 18 Hz) compared with the V2 cells (median 11 Hz). This might seem high compared with earlier studies in V1 and V2 (Foster et al. 1985), but more recent studies in which experimental conditions similar to ours were used have shown that many neurons in V1 (Hawken et al. 1996) and some neurons in V2 (Levitt et al. 1994a) do respond to these relatively high temporal frequencies.

Endstopping

The median stimulus width at which neurons showed their optimal response was 3.2° , which corresponds roughly to the median size that we determined when we plotted receptive fields by hand. About 25% of our sample was strongly endstopped; endstopped neurons typically showed greatest suppression when the diameter of the stimuli exceeded 10° . Few neurons showed larger suppressive surrounds of up to 20° wide.

Contrast response

One of the major differences between parvo- and magnocellular neurons in the lateral geniculate nucleus (LGN) is their contrast response (Kaplan and Shapley 1986). Whereas parvocellular neurons show a linear increase in firing rate with increasing contrast, magnocellular neurons respond nonlinearly. They have a higher sensitivity for contrast and saturate at relatively low contrast levels. We examined the contrast responses of V3 neurons to see whether they would preferentially show one or the other type of behavior. Three examples are illustrated in Fig. 5, A–C. The solid curve shows the best fit of the Naka-Rushton equation given above. Figure 5, D–F, shows the distributions of the semisaturation contrasts, the contrast response exponents, and the sensitivities of all cells. Overall, cells in V3 were highly responsive.

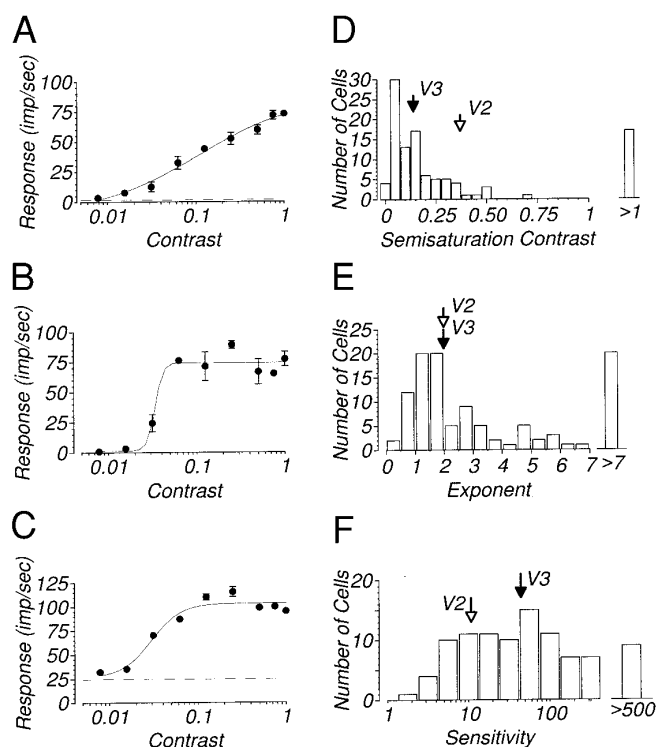


FIG. 5. Characteristics of contrast response in area V3. *A–C*: example contrast response curves. *A*: mostly linear contrast response with a high sensitivity. *B*: highly nonlinear response with a steep threshold between 3 and 5% contrast. *C*: nonlinear contrast response from a highly sensitive neuron. *D–F*: histograms of semisaturation contrasts, contrast response exponents, and contrast sensitivity for 96 V3 cells. Filled arrows: median value of V3 cells. Open arrows: median of the corresponding measure of a sample of V2 neurons at similar eccentricities. *D*: histogram of semisaturation contrasts. *Right*: neurons that did not saturate. *E*: histogram of contrast response exponents. *Right*: cells whose contrast response curve was too steep for a slope to be reliably estimated. *F*: histogram of contrast sensitivities. *Right*: cells that gave a reliable response even to the lowest contrast presented.

The median firing rate in response to a 100% contrast luminance grating was 50 imp/s, with an average baseline response of 3 imp/s. The cell in Fig. 5*A* shows a linear contrast response, albeit on a semilogarithmic scale, and was highly sensitive (sensitivity > 500). The cell in Fig. 5*B* has an extremely steep contrast response and saturates at a low contrast level of ~6%. Its contrast sensitivity could not be determined, because it did not give any spontaneous discharge. The cell illustrated in Fig. 5*C* also has a high contrast sensitivity of 126, but its contrast response curve is less steep and saturates at ~10%–20% contrast. These curves typify the variation of contrast responses observed in V3. We saw essentially every combination of sensitivity and steepness. This is reflected in the wide range of semisaturation contrasts, exponents, and contrast sensitivities, as shown in Fig. 5, *D–F*, respectively. Of these three variables, semisaturation contrast seems to differentiate parvo- and magnocellular responses most reliably (Sclar et al. 1990). The distribution of semisaturation contrasts in Fig. 5*D* seems to reflect input from both types of neurons. Although the peak at low contrasts (0.05) is quite similar to that observed in the magnocellular layers of the LGN, values >20% contrast and the sizeable proportion of nonsaturating neurons seem to

indicate a significant proportion of input from parvocellular neurons (Sclar et al. 1990). Similar distributions for area V1 show a wider spread of semisaturation contrasts (Albrecht and Hamilton 1982; Sclar et al. 1990) that is also present in area V2 (Levitt et al. 1994a).

We compared our data with the results of experiments performed in V2 (Gegenfurtner et al. 1996) and MT (Gegenfurtner et al. 1994; O'Keefe et al. 1993), in which identical methods of animal preparation and visual stimulation were used. The sensitivity of V3 cells is significantly higher than that of V2 cells, and as high or higher than in MT. Median sensitivity for 109 V3 cells was 44.47, which is significantly higher than the median for 49 V2 cells at 10.84 (Mann-Whitney *U* test, $P < 0.001$). Median sensitivity for 62 cells from area MT was 31.37, which was not significantly lower than for V3 (Mann-Whitney *U* test, $P > 0.05$).

Color selectivity

We found that 55 of 102 (53.9%) cells did have $CR > 1.4$. This is close to what was found earlier in area V2 (50%), but significantly above V3 measurements by Felleman and Van Essen (1987), who classified 20% of all cells as color selective. It is well known that color selectivity, probably more than any other measure, depends on the experiments and criteria used for classification (Schein and Desimone 1990). One main reason for the use of the colored bars to define color responsivity was to allow a direct comparison with earlier data from V2 (Gegenfurtner et al. 1996). For many V2 and V3 cells, experiments with isoluminant gratings, or with gratings having a small luminance contrast, did not lead to an accurate classification of color opponency, and often overestimated color opponent inputs. In the experiment with colored bars on a black background, all stimuli have a high luminance contrast, which in the absence of color opponency would saturate the cell irrespective of small deviations from photometric luminance. Only if the cell indeed receives significant color opponent inputs will $CR > 1$. In fact, many cells showed a behavior like that of the cell illustrated in Fig. 3. Had we defined our measure for color responsivity through the experiment with sinusoidal gratings, higher values of CR would have resulted. For example, for the cell from Fig. 3 we would have obtained a value of 3.28 rather than 1.15. There were several cells that showed color selectivity for low-luminance contrast colored gratings, but not for high-luminance contrast colored bars. No cell showed the opposite behavior. Therefore the experiments with the colored bars provide a more conservative criterion for color selectivity than experiments with sinusoidal gratings.

Furthermore, we can be quite sure that chromatic aberration did not play a significant role in this experiment, because any luminance artifacts introduced by chromatic aberration should be negligible compared with the luminance contrast of the stimuli. Also, because we used stimuli at the cells' preferred spatial frequency in these experiments, and because the preferred spatial frequencies of most of the cells we tested were rather low (<2 cycles/degree for 85% of the cells), we are confident that chromatic aberration did not significantly contribute to our results.

However, to allow a better comparison with the results of

Felleman and Van Essen (1987), we computed for the cells in our study the white index and color index those researchers had used. In the experiment with the colored bars on the black background, which was most similar to those of Felleman and Van Essen (1987), 27 of 102 cells (26.4%) had a color index >0.7 , which is quite similar to the 20% found by Felleman and Van Essen. The distribution of color and white indexes we obtained was also quite similar to the one shown in Fig. 14 of Felleman and Van Essen (1987). When we computed the same indexes for the grating experiment, 46 of 71 cells (64%) had a color index >0.7 . Therefore, as already pointed out above, the experiment with the bars on a black background provides for a more conservative measure of color selectivity. One could argue that the criterion value of 1.4 is not very strict, and that maybe many of the cells just fall above it by chance. However, with the use of a stricter value of 2.0, 21 of 102 cells (20.6%) still fell above the criterion, which, once again, closely matches the proportion found in area V2 (25%).

Selectivity to different stimulus attributes

We also investigated the relationships among the tuning characteristics of V3 cells for different stimulus attributes. If different stimulus attributes are processed independently, as has been proposed frequently (DeYoe and Van Essen 1985; Livingstone and Hubel 1988; Zeki 1993), then one might expect neurons to show selectivity primarily to one stimulus attribute, i.e., they should be tuned to direction of motion, or for color, or for form, but not for several attributes simultaneously. We used the results of the experiments described earlier to extract indexes for each cell specifying their selectivity to color, orientation, size, and direction of motion. Figure 6 shows the results of these experiments. No systematic relationship between color and orientation selectivity, endstopping, or directionality was seen in this analysis of V3 cells. Figure 6A shows a scatterplot of ORI and CR for 86 V3 cells. The large filled symbols indicate median values of the indexes for our V3 sample and for a comparable sample of V2 neurons (Gegenfurtner et al. 1996). Almost all neurons (80%) in V3, as in V2, show some degree of orientation selectivity. There is no correlation between selectivity for color and orientation. There exist cells that are highly selective for both color and orientation. Figure 6B shows a similar scatterplot for color and directional selectivity. Once again, there is no systematic relationship between color selectivity and direction selectivity. Cells in V3 are generally more directionally selective than the V2 cells. Figure 6C shows the association between color and endstopping. Many of the highly endstopped cells are also selective to color. The median ES of the V3 cells is lower than for the V2 cells, suggesting a lesser degree of endstopping in V3.

Figure 6, A–C, also indicates that all four indexes are distributed continuously through the V3 sample. Therefore any criterion for classification of cells as selective for a certain attribute is arbitrary. Nevertheless, we used the above mentioned set of criteria, which are also indicated as horizontal and vertical lines in Fig. 6. This allowed us to compute a statistical measure for the degree of association between each pair of stimulus attributes. We used Fisher's exact test

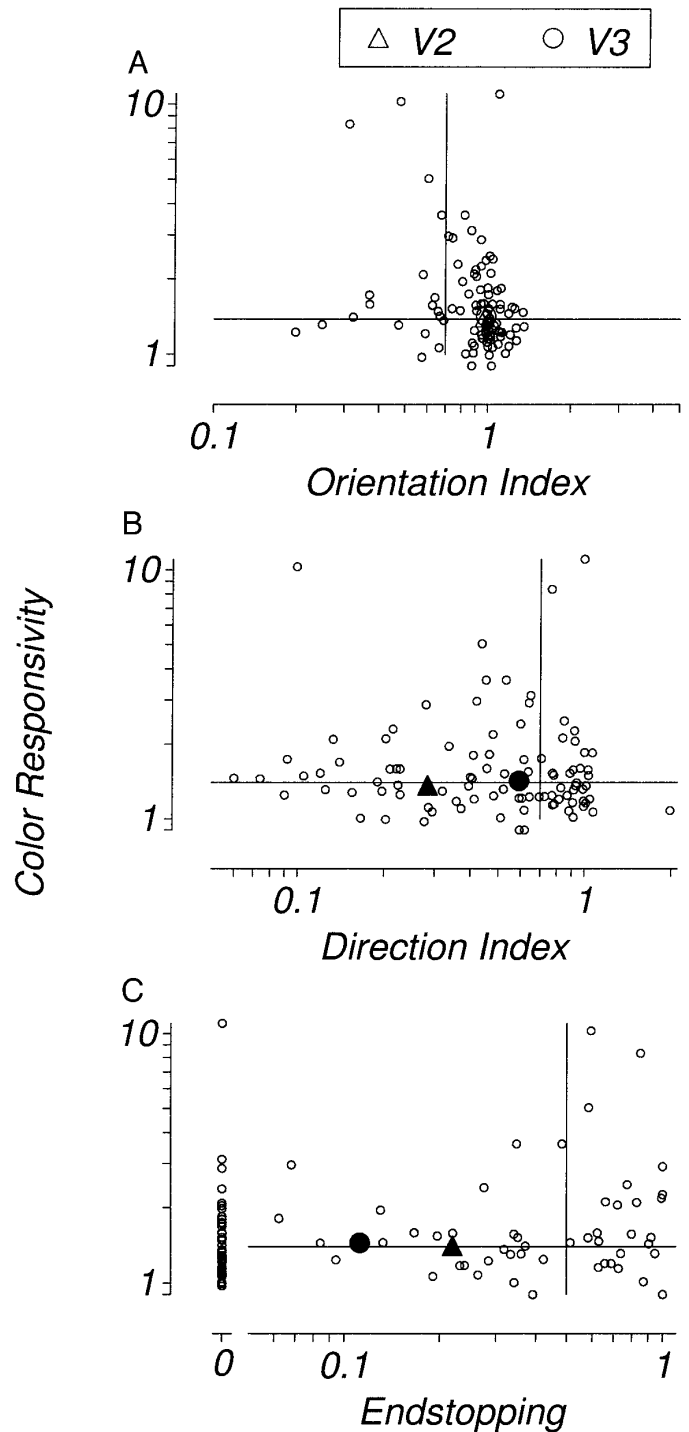


FIG. 6. Association between different response properties. Filled triangle: median observed in a sample of V2 neurons. Filled circle: median for the V3 sample. A: scatterplot of ORI and CR for 97 V3 cells. B: scatterplot of DI and CR for 97 V3 cells. C: scatterplot of ES and CR for 94 V3 cells.

for probabilities (see Hays 1981, p. 552–555) to test the hypothesis that there is an association between different stimulus attributes. Table 1 shows fourfold tables of the occurrences of selectivity of neurons for a certain attribute. The probability of obtaining this particular table, or one that is even more indicative of association given the same marginals, under the null hypothesis of no association, is

TABLE 1. *Incidence of combinations of different attributes*

Attribute (A vs. B)	A and B	A and Not B	Not A and B	Not A and Not B	<i>P</i>
Color vs. direction	15	27	20	23	0.38
Color vs. orientation	39	8	34	4	0.535
Color vs. endstopping	14	31	7	33	0.21

For each pair of attributes (A and B) we show the number of cells selective for A and B, A and not B, not A and B, not A and not B. *P*: probability of obtaining such a 4-way table (or one even more indicative of association) under the hypothesis that there is no association between stimulus attributes A and B, according to Fisher's exact test for probabilities. None of the entries was statistically significant ($\alpha = 0.05$).

indicated in the *right column*. None of the values is statistically significant at the 0.05 level. Therefore we can reject the hypothesis of an association between different stimulus attributes.

In Fig. 6 we used color responsivity to specify the degree of color selectivity of each cell. However, we generally obtained equivalent results, namely a lack of association between color and other stimulus attributes, when we used other indicators for color selectivity. In particular, we looked at color index and white index as defined by Felleman and Van Essen (1987), color responsivity calculated from the results of the experiments with sinusoidal gratings of low luminance contrast, and the elevation of the preferred color direction as defined by Derrington et al. (1984). None of these indicators for color selectivity showed a significant association with orientation, direction, or size selectivity.

In Fig. 7 selectivities for direction, orientation, color, and size are compared between areas V2 and V3. The V2 data are from a comparable sample of cells (Gegenfurtner et al. 1996), with the use of the same criteria as here for classification. There is little difference between V2 and V3, with the exception that a significantly larger proportion of V3 cells (40%) shows direction selectivity. As in V2, most cells in V3 are orientation selective, and there is a relatively high degree of color selectivity in both areas. Interestingly, the proportion of endstopped cells is about equal in both areas,

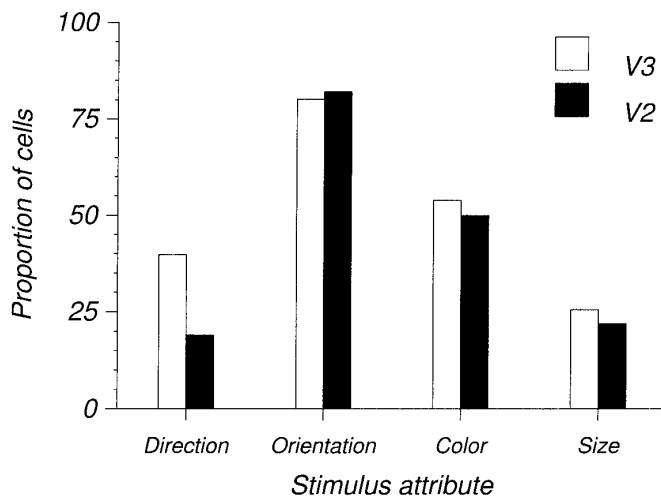


FIG. 7. Comparison of the tuning characteristics of V2 cells and V3 cells. V2 data are from Gegenfurtner et al. (1996), and are from all 3 cytochrome oxidase (CO) compartments of V2. In both samples cells with $DI > 0.7$ were classified as directionally selective; cells with $ORI > 0.7$ were classified as orientation selective. Cells with $CR > 1.4$ were classified as color selective. Cells with $ES > 0.5$ were classified as being endstopped (selective to size).

even though the median value for endstopping is higher in V2, as shown in Fig. 6. This is because of the larger number of neurons in V3 that do not show any endstopping at all.

Color tuning

Even though the proportion of color cells is about equal in areas V2 and V3, we found large qualitative differences in the cells' responses to color. Most prominently, there was a large proportion of V3 cells that showed significant input from the S cones. Also, as seen above, we did find a significant proportion of color-selective cells in V3 that also showed strong selectivity to direction of motion. An example cell, combining both of these features, is shown in Fig. 8.

Figure 8A shows responses to isoluminant blue and yellow sinusoidal gratings of different orientations. Even though the cell did give a strong response at all orientations, there is a marked peak at $\sim 45^\circ$. The response in the direction opposite the maximum is also attenuated, resulting in a strong directional selectivity. Figure 8, B and C, shows the spatial and temporal frequency tuning, respectively, for the same cell, measured with the same isoluminant blue and yellow grating. There is a preference for very low spatial frequencies, with essentially no response at > 0.5 cycles/degree. However, the temporal frequency response peaks at ~ 10 Hz and the cell responds quite briskly to rather high temporal frequencies (~ 30 Hz). Interestingly, at 30 Hz the isoluminant blue and yellow grating is hardly visible to the human observer. This was not an isolated example. Many cells showed a good response to isoluminant gratings, even at high temporal frequencies. The majority of these cells, however, had only weak S cone inputs. For these we typically found that there would be a null response close to, but not exactly at, photometric isoluminance. The experiment we used to test for such a null response is illustrated in Fig. 8D. We compared responses to achromatic black-and-white gratings of increasing luminance contrast with the responses of chromatic gratings of the same luminance contrast. In Fig. 8D, for example, the circles indicate responses to the achromatic gratings and the triangles indicate responses to blue and yellow chromatic gratings whose luminance contrasts were matched to that of the achromatic gratings. For the cell shown in Fig. 8D, it is clear that the response does not null at any luminance ratio of blue and yellow bars, not even when they are isoluminant. This cell, therefore, has a significant color opponent input from the S cones. But note that it also gives a strong response to the black-and-white stimuli. Most cells, however, had only a weak S cone input that was added to strong, additive L and M cone inputs.

Even though we found a significant number of cells that

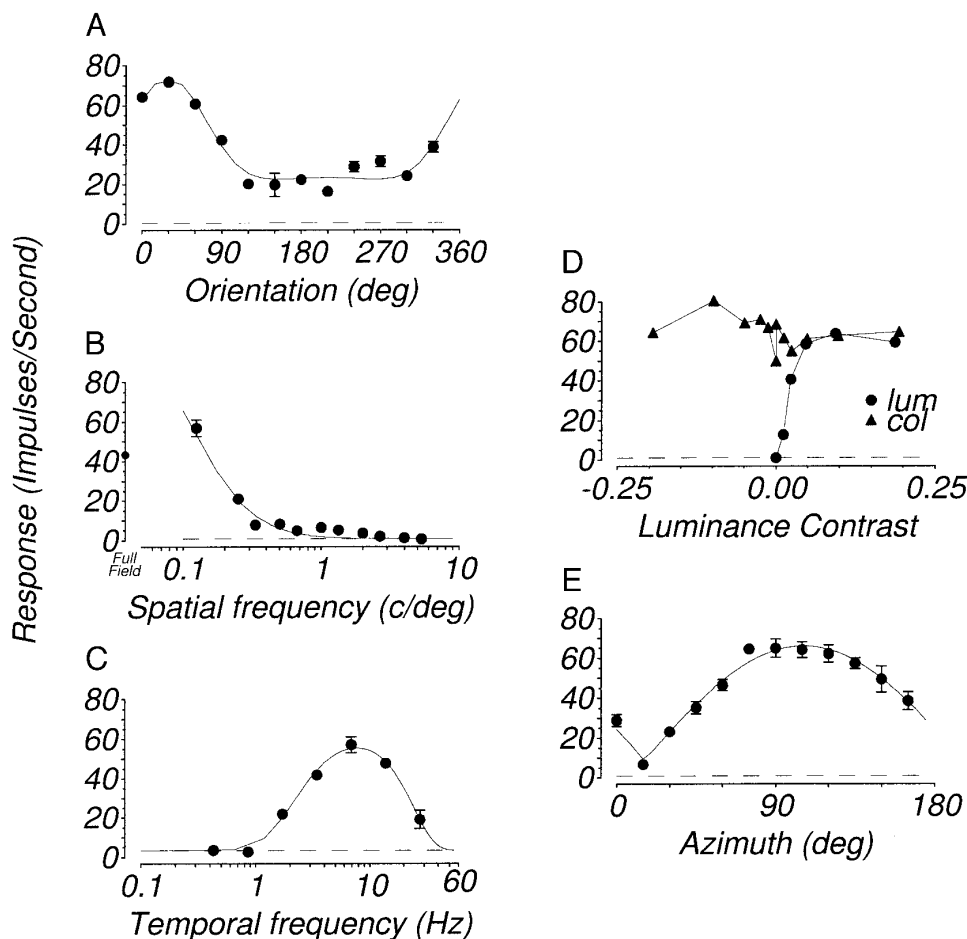


FIG. 8. Example of a cell showing high selectivity to blue/yellow color modulations and to direction of motion. *A*: responses to blue/yellow isoluminant sinusoidal gratings of different orientation and direction. *B*: responses to blue/yellow isoluminant sinusoidal gratings of different spatial frequencies. *C*: responses to blue/yellow isoluminant sinusoidal gratings of temporal frequencies. *D*: responses to sinusoidal gratings of different luminance contrast. Circles: responses to black-and-white gratings. Triangles: responses to blue and yellow gratings. Positive contrasts are for gratings in which the blue bars were brighter than the yellow ones; negative contrasts are for the opposite case. *E*: responses to isoluminant gratings along the color directions shown in Fig. 2.

behaved this way, the majority of cells showed a response null within $\pm 5\%$ luminance contrast of the photometric isoluminant point. We further investigated the chromatic tuning of this cell with isoluminant grating stimuli modulated in 12 different color directions. Figure 8*E* shows that the results are very orderly. The responses are well predicted by a linear combination of cone inputs, shown by the solid sinusoidal curve. The response is best at an azimuth of $\sim 105^\circ$, which is very close to the direction (90°) that differentially excites the S cones. As predicted by the model, there is a complete response null at an azimuth of 15° , close to the L-M color opponent direction.

Figure 8*E* indicates an excellent fit of the linear model that was first proposed by Derrington et al. (1984). Specifically, the model predicts that the response R in a color direction with elevation ($elev$) and azimuth (az) is given by

$$R = b + A|\sin(elev)\sin(\Phi) + \cos(elev)\cos(\Phi)\cos(az - \Psi)|$$

where b is the response baseline, A is the maximum response amplitude, ϕ is the cell's preferred elevation, and Ψ is its preferred azimuth. We tested this model on 81 cells with the use of the stimuli described in Fig. 2*A*. All stimuli had a 10% luminance contrast and their azimuth varied in equally spaced steps of 30° . In addition to those chromatic stimuli, we used an achromatic black-and-white grating with the same luminance contrast of 10%. For all cells the model provided a reasonably good fit to the data. The example

shown in Fig. 3*D* gives an illustration of the typical quality of the fits.

Figure 9*A* shows the preferred elevations and azimuths estimated by the model. Because most cells responded well to luminance stimuli, the elevations are generally quite high, $\geq 60^\circ$. Only a few cells did not respond well to the achromatic stimulus. Figure 9*B* shows a histogram of the preferred azimuths shown in Fig. 9*A*. Many cells had a preferred azimuth of $\sim 270^\circ$ ("blue"), indicating at least some S cone input. A fair proportion of cells was tuned to other color directions, except for a striking gap at an azimuth of 90° . This is surprising because in most other areas of visual system, especially in the LGN (Derrington et al. 1984), only a minority of cells is tuned to the blue/yellow color direction.

Figure 9*B* also shows that there is no correlation of V3 cells' preferred color directions and the perceptually defined "unique hues" (Jameson and Hurvich 1955). The arrows in Fig. 9*B* indicate the directions of the unique hues for the stimuli we used, as determined by visual inspection. There is no clustering of preferred azimuths around those directions. Neither is there a strong preference for the "cardinal directions," as was observed in the LGN (Derrington et al. 1984). Except for the imbalance between blue and yellow, the preferred azimuths are fairly evenly distributed around color space.

Pattern motion

As shown before, the major difference between V2 and V3 is a considerable increase in directional selectivity in

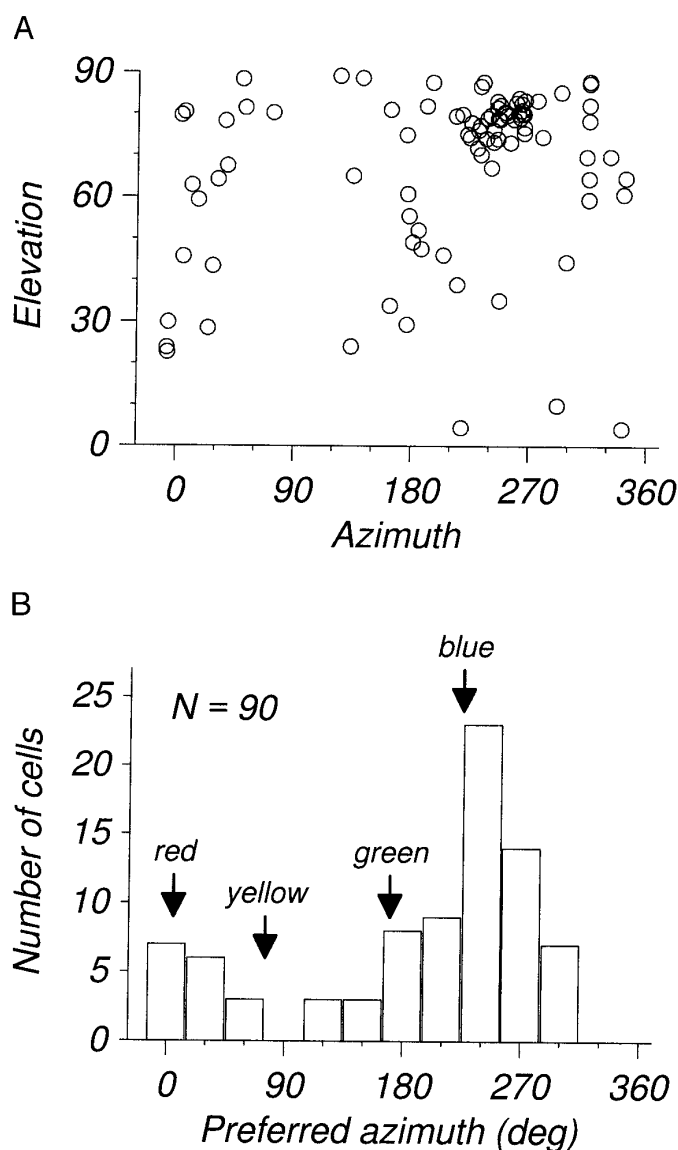


FIG. 9. A: preferred azimuths and elevations of 90 V3 cells. Because the sinusoidal gratings were modulated symmetrically around the white point of our color space, only positive elevations are shown. B: histogram of preferred azimuths of 83 V3 cells. Arrows labeled red, yellow, green, and blue: color directions roughly corresponding to "unique hues" or "pure colors" for the human observer.

V3. About 40% of all V3 cells showed strong directional selectivity (V2: 19%). This is higher than in any other area of visual cortex, except for area MT, where ~90% of all cells are strongly directional (Albright 1984; Dubner and Zeki 1971). A major input for V3 comes from cells in layer 4B of V1, from which a significant portion of MT's input also originates. There are also significant projections from area V3 to MT. Therefore we investigated whether V3 might play a role in the transformation of visual motion signals.

One of the distinctive features of area MT is the presence of a proportion of cells that responds to feature motion. When two drifting sinusoidal gratings at different orientations are superimposed, the resulting plaid pattern (Movshon et al. 1985) appears to move coherently in the direction in which the intersections of the gratings bars move. Whereas

directionally selective cells in areas V1 and V2 give a response to such plaids only when one of the components moves in the cells' preferred direction, there are cells in area MT that will respond when the plaid pattern moves in the cells' preferred direction (as determined with a single grating). The former type of cell is called a "component cell," the latter a "pattern cell." About 15% of all MT cells are classified as being pattern cells. In V1, on the other hand, there are no pattern cells (Movshon et al. 1985).

Figure 10 shows some examples of response patterns we found in area V3. The responses are shown for single gratings (filled circles: component) as a function of the grating orientation. The responses to plaids (open squares) are plotted as a function of the orientation perceived by the observer. In this case we used two sinusoidal gratings at a relative orientation of 120° . The resulting direction of the pattern motion is in this case equal to the vector sum of both components at the intermediate angle. For example, the plaid orientation of 180° would correspond to the components moving at angles of 120° and 240° . For pattern cells we would predict the response to the plaid to be proportional to the response to a single grating moving in the pattern direction. Therefore the prediction for the response to the plaid is not shown separately in the Fig. 10, because it is equal to the component response. If a cell responded to the components alone, the response to a plaid should be proportional to the sum of the responses to the plaid components. This component prediction is shown by the open triangles in Fig. 10. By comparing the plaid and component predictions in Fig. 10, it becomes apparent that the two sets of predictions are typically correlated. As described previously (Movshon et al. 1985), we computed the correlation between plaid response and plaid prediction, after partialing out the component prediction and vice versa (see Hays 1981). Because correlation coefficients are independent of scaling or shifting the response curves, we can ignore the problem of normalizing the responses to components and plaids. We ran this experiment on 39 cells that were at least directionally biased, and that we could hold long enough.

The cell in Fig. 10A shows a relatively broad orientation tuning. Its tuning is almost identical for single gratings and plaids. There is a high correlation between plaid prediction and the actual responses to plaids, and a negative correlation between plaid responses and the component predictions. Therefore we can classify this cell as a pattern cell. In fact, this cell is a rather rare example of a pattern cell that does not give any response to the components of the plaid. For example, when the plaid moves at an orientation of 270° , one of the components moves at an orientation of 210° , which is the cell's preferred orientation. Still, in the presence of the other component at an orientation of 330° , the response is completely abolished. We were able to classify 3 of the 39 cells on which we ran this experiment as pattern cells. This might seem a small number, but one should bear in mind that even in area MT there are only ~15% pattern cells.

There are also many cells that have a high correlation both with the plaid and the component prediction. An example of such a cell is shown in Fig. 10B. Its orientation tuning is very broad, and the plaid and component predictions are actually quite similar. Cells such as this one cannot be readily

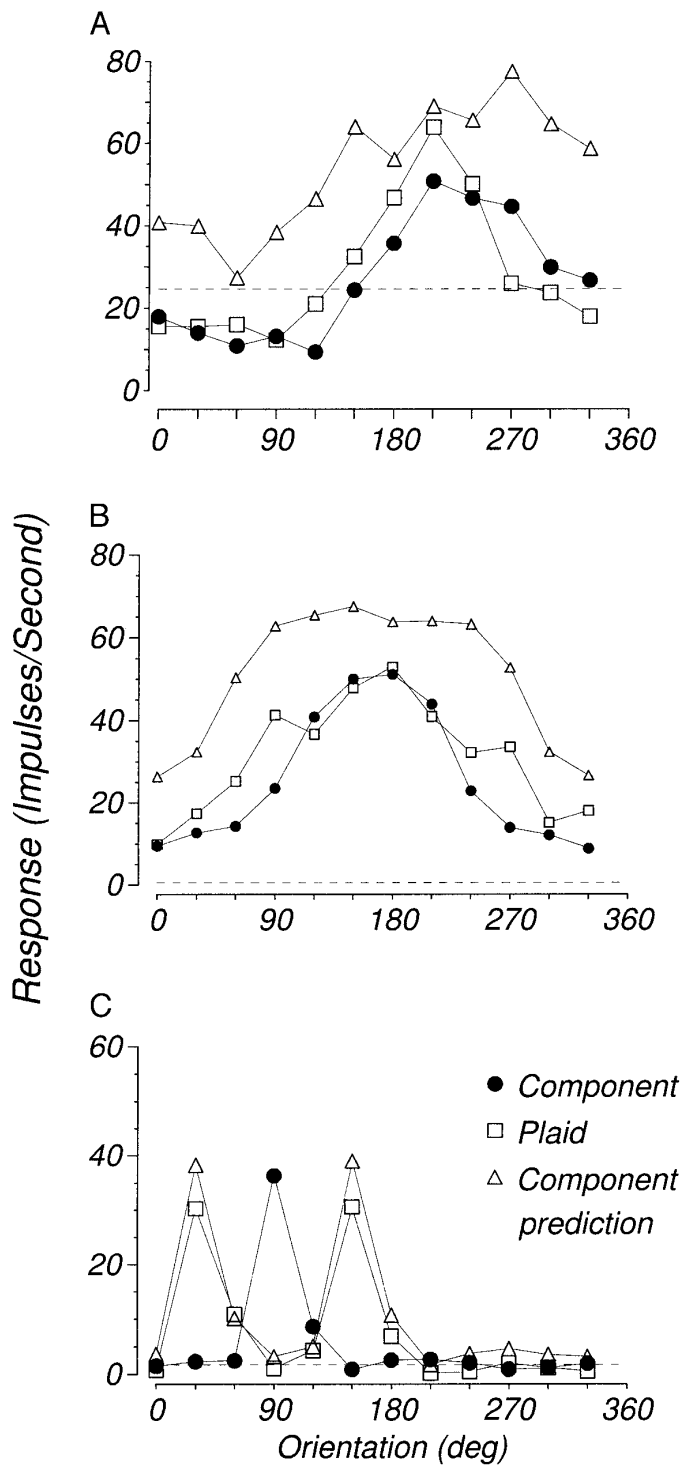


FIG. 10. Examples of responses to plaid stimuli. Filled circles: responses to single sinusoidal gratings. Open squares: responses to pairs of gratings with orientations 120° apart. Orientation in this case means the average orientation of the 2 gratings, which is the direction in which human observers typically see these patterns move. Open triangles: prediction of the cell's responses on the basis of the component response alone. *A*: pattern cell. Plaid response and component prediction are very similar, and different from the component response. *B*: unclassified cell. Correlations are high for this cell between all 3 sets of data points. *C*: component-selective cell. There is a high partial correlation between the plaid response and the component response, but not between the plaid response and the component prediction.

TABLE 2. Proportion of cells in areas V1, V3, and MT of macaque monkeys selective to pattern or component motion, or equally to both

Area	Pattern	Unclassified	Component	Number of Cells
V1	0	16	84	69
V3	7.6	41	51.4	39
MT	15.2	40	44.8	118

Unclassified: cells selective equally to pattern and component motion. Numbers for V1 and MT cells are from Movshon et al. (1985). MT, middle temporal area.

classified as either type, but they do give a good response in the pattern direction. In fact, 30.7% (12 of 39) of all cells had their response peak to plaids in the pattern direction. Therefore the type of cell illustrated in Fig. 10B could well be the precursor for a "true" pattern cell. In MT, there are many unclassified cells, $\sim 40\%$, and we found an equal proportion of cells in V3 (41%) showing that type of behavior. In area V1, on the other hand, as shown in Table 2, there are only 16% unclassified cells. It is instructive also to look at the pattern correlation by itself. About a third of MT cells (35.2%) show a strong partial correlation between plaid responses and pattern prediction. In V3 this percentage is just as high (38.5%), whereas it is negligible in V1 (4.3%).

Finally, Fig. 10C shows a component cell. Component cells typically have a narrower orientation tuning curve, and the plaid responses show two distinct peaks. Of the 39 directionally selective cells in our sample, 20 (51.4%) were component cells. This proportion is slightly higher than in MT (44.8%).

Figure 11 shows a scatter plot of component and pattern correlations for all 39 V3 cells. The solid curves divide the

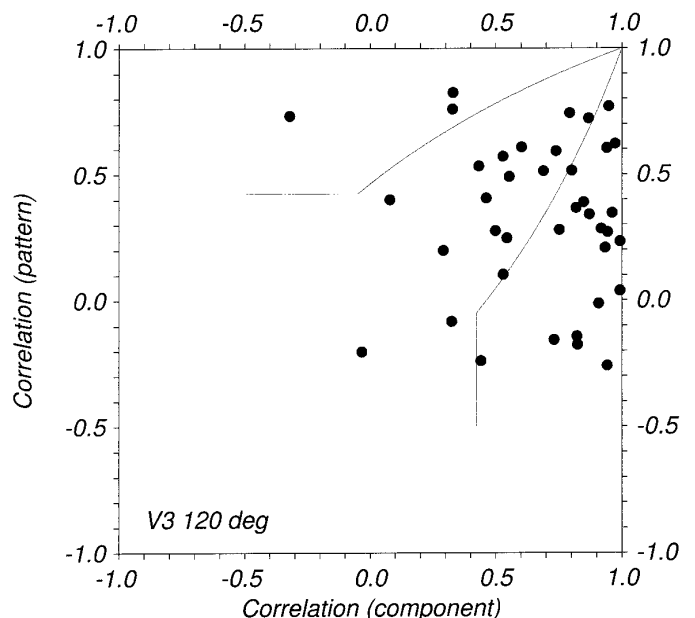


FIG. 11. Plaid and component correlations for 39 directionally selective V3 cells. Filled symbols: for each cell, the partial correlation of component prediction and plaid response (X-axis) and the partial correlation between component response and plaid response (Y-axis).

area into pattern (*top*), component (*right*), and unclassified cells. This plot is quite distinct from similar plots for area V1 (Movshon et al. 1985). Clearly, there are fewer pattern cells than in area MT, but the high proportion of cells that does actually respond to the pattern motion makes it likely that area V3 plays an important role for such mechanisms.

Laminar distribution

So far we have treated area V3 as one homogeneous area. Although so far no distinct horizontal anatomic subdivisions have been found, such as the cytochrome oxidase blobs in V1 or stripes in V2, it is of great interest to investigate the properties of cells in the different layers of V3. In particular, differences in tuning characteristics between input and output layers can point to the signal transformations that take place in a particular area. For a subset of 125 cells we were able to determine the exact laminar position. Figure 12 shows histograms of the ORI, DI, and ES for the different laminae. We grouped layers 1–3 into superficial layers, layer 4 into the middle layer, and layers 5–6 into deep layers. No substantive differences were found between the tuning properties within these groups.

Figure 12A shows that there were no differences in orientation selectivity among the different layers. This is not surprising, because most V3 cells are orientation selective, as are most cells at preceding stages of cortical processing. Figure 12B shows directional selectivity for the three different groups of layers. There seems to be a tendency for cells in the deep layers to be either strongly directionally selective or not to be directionally selective at all. This was the case both in layer 5 and in layer 6. We could not find any other characteristics that would further differentiate between these two groups of cells. In the superficial layers, directional selectivity was evenly distributed. In the middle layer, the input layer, very little strong directional selectivity is observed, which suggests that this property might actually emerge within area V3. This is the case even though many cells in layer 4B of V1 are strongly directionally selective (Hawken et al. 1988), and many of these cells project to area MT (Movshon and Newsome 1996). Therefore different subpopulations of V1 neurons might project to areas V3 and MT. Figure 12C shows the distribution of ES. Strong endstopping was found only in the superficial layers, and neither in deep nor middle layers.

DISCUSSION

Our results show that neurons in area V3 display an abundance of functional properties. Almost all cells showed orientation selectivity, but directional selectivity, color selectivity, or endstopping were quite common as well. Furthermore, all combinations of tuning characteristics with these attributes were observed. This suggests that the processing of color, form, and motion does not follow segregated pathways within V3.

We also found evidence for mixing of parvo- and magnocellular LGN signals in V3. Contrast sensitivity of V3 cells was extremely high. We note that this by itself could equally reflect a predominance of magnocellular inputs to V3 cells (which are provided by the area V1 layer 4B projections to

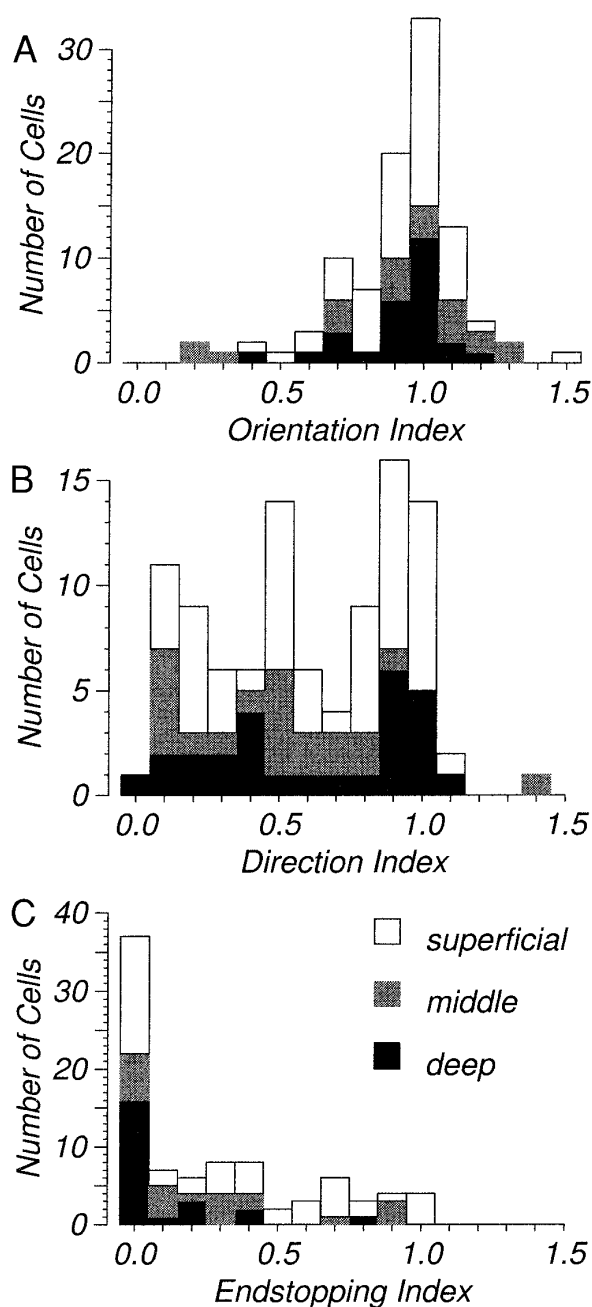


FIG. 12. Laminar distribution of response properties. Black areas: cells from the deep layers. Gray areas: cells in layer 4. White areas: cells in the superficial layers. A: ORI ($N = 99$; deep 27, middle 21, superficial 51). B: DI ($N = 99$; deep 27, middle 21, superficial 51). C: ES ($N = 88$; deep 23, middle 21, superficial 44).

V3) (Felleman and Van Essen 1984) or simply summation of less sensitive V1 or V2 inputs in V3's larger receptive fields. However, we also observed cells with a linear contrast response, which is more typical for the parvocellular pathway (Kaplan and Shapley 1986). The high degree of color selectivity and color opponency also point to a significant parvocellular input to area V3.

Several properties related to higher-level motion analysis first appear in area V3. First, we observed cells that showed strong directional selectivity as well as color opponency, and thus gave strong directional responses to isoluminant

stimuli. Because we could not find cells of this type in area MT (Gegenfurtner et al. 1994) or in area V2 (Gegenfurtner et al. 1996), it is likely that processing of isoluminant motion stimuli takes place in a pathway including V3 and possibly V4. Second, we found directionally selective cells in V3 tuned to the direction of motion of plaid patterns, rather than to the direction of motion of the individual grating components. The proportion of pattern cells in V3 is intermediate between that in V1 (where there are none), and MT (in which roughly 15% are pattern cells). V3 might therefore play an important role in developing pattern motion selectivity. It also appears that these properties are generated within V3 from its V1 inputs, rather than as a result of its V2 inputs. Cells in V3 prefer higher temporal frequencies than cells in area V2. In addition, their color properties are more similar to those in V1 than in V2.

Comparison with other studies

In this study we found that ~85% of the V3 population is orientation selective, 40% directionally selective, roughly 50% color selective, and 25% size selective (i.e., end-stopped). Earlier studies of functional properties of V3 neurons were mainly restricted to determining the proportion of neurons selective for particular stimulus attributes (Baizer 1982; Van Essen and Zeki 1978; Zeki 1978a,b). These studies found direction selectivity to be relatively rare (<15%), and overt color opponency to be completely absent in V3. Differences between the other researchers' results and our own presumably reflect different measurement techniques and the different classification criteria used. The most extensive investigation of functional properties of V3 neurons so far is the work by Felleman and Van Essen (1987), who studied the selectivity of V3 neurons to stimulus wavelength, disparity, size, orientation, and direction. Where our experiments overlap with theirs, there is remarkable agreement. Felleman and Van Essen reported that most V3 cells (76%) were orientation selective [in good agreement with earlier reports by Zeki (Van Essen and Zeki 1978; Zeki 1978a,b) that 70–80% of V3 neurons were orientation selective], 40% were directionally selective, and 20% were endstopped. The proportion of color-selective cells reported by Felleman and Van Essen (20%) was lower than ours, which is again probably due to the different criteria and experiments employed. We did not test responses to stimuli of different disparities, but found that almost all neurons were driven well either monocularly or binocularly at zero disparity. There is one aspect of the Felleman and Van Essen study that we were unable to replicate. Felleman and Van Essen found a small proportion of neurons that had multi-peaked orientation tuning curves, with peaks in nonaligned orientations. We did not observe any such cells. All cells in our sample had either only one peak (directional cells) or two peaks 180° opposite of each other. This difference could be due to the flashed stimuli used by Felleman and Van Essen, because we only used moving gratings. Alternatively, because Felleman and Van Essen found very few such cells, we could have simply missed them.

Motion pathways

The processing of visual motion is generally assumed to take place within the magnocellular pathway. This view has

to be reconsidered, however, because recent evidence suggests that information about certain types of stimulus motion (e.g., color, 2nd order) is unlikely to be processed by area MT. MT neurons exhibit only poor sensitivity to such stimuli (Dobkins and Albright 1994; Gegenfurtner et al. 1994; O'Keefe et al. 1993; Shadlen et al. 1993). Lesion studies (Merigan et al. 1991) have also shown that there is no deficit in the perception of slowly moving patterns after magnocellular LGN lesions. Similarly, the well-known "motion-blind" patient of Zihl with bilateral lesions to the posterior temporal cortex, including the human analogue of area MT, showed little or no deficit when tested with slowly moving stimuli (Hess et al. 1989; Zihl et al. 1983). Another cortical pathway seems to underlie perception of these types of stimuli. Area V3 is an ideal candidate to perform this task, with its high proportion of directionally selective cells that are sensitive to other stimulus attributes. Consistent with this, Shipp et al. (1994) conducted a positron emission tomography study on the above mentioned patient, and reported residual activity to moving stimuli in area V3.

Our results also suggest that area V3 might be an important site for the development of pattern motion selectivity. Cells exist in V3 that are pattern selective only, but there is also a greater number of cells that respond to the pattern motion as well as the component motion. Often these cells give the largest response in the pattern motion direction. Any subsequent narrowing of the orientation tuning would turn them into true pattern-selective cells. There are several motion models that assume two separate pathways to area MT (e.g., Wilson and Kim 1994). One is direct and is for processing first-order motion energy. The second is via a second stage, often assumed to be area V2, and is for processing more complex motion stimuli such as plaids or drift-balanced second-order stimuli (Chubb and Sperling 1988). Our results indicate that V3 is a more likely candidate for this secondary motion area, because some cells in V3 do indeed respond to pattern motion. No systematic study of pattern motion selectivity in area V2 is known to us, but our own informal observations on a large number of cells did not give any evidence for pattern cells in area V2. Much less is known about the processing of second-order motion stimuli. Our own informal observations on cells in V2 and V3 suggest that neither area gives significant responses to drift-balanced stimuli. Whether area MT actually responds to these types of motion stimuli is currently a matter of debate (Albright 1992; O'Keefe et al. 1993; Shadlen et al. 1993).

Motion perception at isoluminance

Recent psychophysical experiments on color and motion have made it clear that the motion system as a whole is far from being color blind, as was initially thought. On the contrary, under certain viewing and stimulus conditions (foveal viewing, slowly moving targets), sensitivity to isoluminant red/green gratings can be much higher than to luminance-defined targets (Derrington and Henning 1993; Gegenfurtner and Hawken 1995; Metha et al. 1994; Stromeyer et al. 1995). Furthermore, these targets are detected by a chromatically opponent mechanism whose characteristics are quite different from those of neurons along the magnocel-

lular pathway, for example in area MT (Dobkins and Albright 1994; Gegenfurtner et al. 1994; Saito et al. 1989). The neural substrate for the detection of these stimuli therefore has to combine different properties, in this case color and motion, instead of processing them separately and independently. There is already a large degree of mixing of different signals across the different CO compartments of area V2 (Gegenfurtner et al. 1996; Levitt et al. 1994a; Peterhans and von der Heydt 1993). Our data show that this is even more prominent in area V3, and that there exist many cells that give directional responses to isoluminant stimuli. One characteristic of psychophysical responses to such isoluminant motion stimuli is the high sensitivity at low temporal frequencies. Interestingly, neurons in area V3 have a very broad temporal frequency tuning, and respond briskly even at low temporal frequencies, unlike neurons in area MT. The pathway via areas V3 and V4 might therefore be a suitable candidate to underlie the perception of motion of slowly moving isoluminant stimuli.

S cone pathways

An intriguing aspect of our data is the high proportion of neurons with a significant S cone input. In most visual areas, cells tuned to the red/green color direction are much more common than blue/yellow cells (Derrington et al. 1984; Lennie et al. 1990). In V3 this was not the case. We observed many neurons not only responding to isoluminant blue/yellow stimuli, but doing so even at high temporal frequencies of ~30 Hz, at which these stimuli were hardly visible to the human eye. It was previously assumed that the S cone pathway had a slow temporal response (Green 1968; Kelly 1974), but recent work by Stockman et al. (1993) has very elegantly shown that there also is a fast S cone pathway.

For a few cells in our sample, the S cone input was to a blue/yellow color opponent channel. Those cells would respond at all luminance ratios of blue and yellow lights, but not to red/green modulations. The majority of cells with an S cone input, however, showed a null close to photometric isoluminance. All of these cells responded better to blue than to yellow, and nulled when the blue bars of a grating were darker than the yellow bars. Because this behavior is highly unusual, we thought about several other explanations that could lead to an imbalance between yellow and blue.

After carefully checking the calibration of our monitor and making sure that the yellow and blue bars of our sinusoidal gratings indeed had the same photometric luminance, we investigated whether macular pigmentation, or other differential absorptions of the optical media, could produce such a tuning. However, this is very unlikely for the following reasons.

1) Any such effect would be visible at earlier stages of processing, for example the LGN or V1. No preference for blue has been reported for either LGN (Derrington et al. 1984) or V1 (Lennie et al. 1990).

2) The macular pigment has its highest density within a radius of roughly 1.5° of the fovea (see Wyszecki and Stiles 1982). Although we had some foveal cells, the majority of cells was located $2-5^\circ$ away from the fovea. Any differential absorption of short-wavelength light by the macular pigment would not affect these cells.

3) Most importantly, the macular pigment absorbs short-wavelength light preferentially. That means that the S cone input is attenuated, and the responses should therefore be smaller to blue than to yellow. We observe exactly the opposite, an enhanced response to blue.

We can also exclude a significant intrusion from the rod photoreceptors. When the pupils are fully dilated, we estimate retinal illumination at ~800 photopic trolands, which is well in the saturating range of the rods (see Wyszecki and Stiles 1982). Also, the peak scotopic wavelength sensitivity occurs at ~507 nm, which corresponds to an azimuth of ~ 170° .

Therefore we feel quite confident that the preference for short-wavelength light of many of the cells in our sample actually reflects S cone inputs to these cells. However, one has to keep in mind that this S cone input is still small compared with the L and M cone inputs these cells receive. It simply reflects a small contribution of the S cones to the luminance-based responses of these cells, and is therefore in agreement with psychophysical results (Stockman et al. 1991) showing an S cone contribution to the luminance pathway. In the psychophysical experiments the S cone input reversed its sign at high temporal frequencies, but unfortunately we ran the color tuning experiments only at one temporal frequency.

Cortical hierarchies

Most corticocortical anatomic connections are compatible with a processing hierarchy that proceeds from V1 through V2 and V3 and then splits into temporal and parietal streams. Some receptive field properties are compatible with this hierarchical organization. For example, receptive field sizes tend to increase at later stages, with V1 fields smallest and fields in MT or V4 being larger. This indicates summation processes over a large number of cells at earlier levels. V3 receptive fields are also larger on average than V2 fields (Felleman and Van Essen 1987; Gattass et al. 1988), in accordance with a hierarchical model.

However, there are several aspects that seem to contradict a simple hierarchical processing scheme via V2 and V3. First, V3 cells are tuned to higher temporal frequencies and have higher temporal frequency cutoffs than V2 cells. Simple averaging of cells at earlier levels would predict lower temporal frequency preferences, for example as is observed when going from the LGN to V1. A substantial proportion of cells in V3 is tuned to temporal frequencies to which no cells in V2 respond. These cells presumably receive their inputs directly from some other preceding cortical area. Most likely this is layer 4B of V1, which has strong projections directly to V3 (Felleman and Van Essen 1984). It is reasonable to suggest that there are functionally distinct V1 projections to V2 and V3. Levitt et al. (1994b) showed that the V1 layer 4B projection to V2 arises from pyramidal neurons, whereas the projection to MT from the same layer is provided by the spiny stellate cell population (Shipp and Zeki 1989). Furthermore, V3 has no strongly directionally selective cells in the input layer 4, whereas V2 has many (Levitt et al. 1994a). This suggests that this property is created *de novo* within area V3, rather than from the same class of inputs as V2. Finally, the color properties of V3 cells are

very much like what is observed in V1. Responses to chromatic stimuli are well described by a model linearly combining cone inputs. In V2, about a third of the cells have a nonlinear tuning to specific color and luminance combinations (Gegenfurtner et al. 1993). We did not observe that type of behavior in V3. Therefore it seems likely that V3 actually receives its largest input directly from V1, rather than from the preceding stage, area V2. This leaves open the intriguing question of the functional relevance of the V2 inputs to V3.

Our results show a substantial chromatic signal in area V3. This might seem puzzling given V3's place in a pathway nominally dominated by signals from the magnocellular layers of the LGN, which show no color opponent behavior. We are therefore left to explain the source of this signal. Felleman and Van Essen (1984) reported that the projection to V3 from V1 arose essentially exclusively from layer 4B, which is dominated by LGN magnocellular inputs via layer 4C α . However, it has long been suspected that 4B neurons could have access to parvocellular signals via their apical dendrites in layer 3 (Lund 1973). Sawatari and Callaway (1996) recently used laser photostimulation of cortical slices to show that there are indeed parvocellular inputs to layer 4B. Alternatively, the chromatic properties we described here in V3 might derive from its inputs from the upper layers of V2, or from the less direct projection from the upper layers of V1.

Conclusions

Essentially all V3 neurons are orientation selective and respond over a broad range of temporal frequencies. Area V3 seems to play an important role in the processing chain of motion and color stimuli. It has a prominent population of directionally selective neurons, and several forms of higher-order motion processing appear in V3 for the first time in the central visual pathways. The types of contrast response behavior and chromatic selectivities that are observed also suggest that V3 plays an important role in integrating parvo- and magnocellular signals. All of the higher-level motion properties that we have described seem consistent with the suggestion of Zeki (1993) that V3 is important for dynamic form analysis.

We thank D. Braun, S. Fenstemaker, M. Hawken, and J. Lund for valuable discussions and for comments on an earlier draft of this paper. We are grateful to Janssen Pharmaceutical for the gift of sufentanil citrate.

This work was supported in part by Medical Research Council Grant G9203679N and National Eye Institute Grant EY-10021 to J. S. Lund, and by a grant from the ARC program of the Deutscher Akademischer Austauschdienst and the British Research Council. K. R. Gegenfurtner was supported in part by a travel fellowship from the SmithKline Beecham Foundation.

Address for reprint requests: K. R. Gegenfurtner, Max-Planck-Institut für Biologische Kybernetik, Spemannstr. 38, 72076 Tübingen, Germany.

Received 31 May 1996; accepted in final form 2 December 1996.

REFERENCES

- ALBRECHT, D. G. AND HAMILTON, D. B. Striate cortex of monkey and cat: contrast response function. *J. Neurophysiol.* 48: 217–237, 1982.
- ALBRIGHT, T. D. Direction and orientation selectivity of neurons in visual area MT of the macaque. *J. Neurophysiol.* 52: 1106–1130, 1984.
- ALBRIGHT, T. D. Form-cue invariant motion processing in primate visual cortex. *Science Wash. DC* 255: 1141–1143, 1992.
- BAIZER, J. S. Receptive field properties of V3 neurons in monkey. *Invest. Ophthalmol. Visual Sci.* 23: 87–95, 1982.
- BARLOW, H. B., BLAKEMORE, C., AND PETTIGREW, J. D. The neural mechanism of binocular depth discrimination. *J. Physiol. Lond.* 193: 327–342, 1967.
- BURKHALTER, A., FELLEMAN, D. J., NEWSOME, W. T., AND VAN ESSEN, D. C. Anatomical and physiological asymmetries related to visual areas V3 and VP in macaque extrastriate cortex. *Vision Res.* 26: 63–80, 1986.
- CHUBB, C. AND SPERLING, G. Drift-balanced random stimuli: a general basis for studying non-Fourier motion perception. *J. Opt. Soc. Am.* 5: 1986–2007, 1988.
- DERRINGTON, A. M. AND HENNING, G. B. Detecting and discriminating the direction of motion of luminance and colour gratings. *Vision Res.* 33: 799–811, 1993.
- DERRINGTON, A. M., KRAUSKOPF, J., AND LENNIE, P. Chromatic mechanisms in lateral geniculate nucleus of macaque. *J. Physiol. Lond.* 357: 241–265, 1984.
- DEYOE, E. A., HOCKFIELD, S., GARREN, H., AND VAN ESSEN, D. C. Antibody labeling of functional subdivisions in visual cortex: Cat-301 immunoreactivity in striate and extrastriate cortex of the macaque monkey. *Visual Neurosci.* 5: 67–81, 1990.
- DEYOE, E. A. AND VAN ESSEN, D. C. Segregation of efferent connections and receptive field properties in visual area V2 of the macaque. *Nature Lond.* 317: 58–61, 1985.
- DOBKINS, K. R. AND ALBRIGHT, T. D. What happens if it changes color when it moves?: the nature of chromatic input to macaque visual area MT. *J. Neurosci.* 14: 4854–4870, 1994.
- DUBNER, R. AND ZEKI, S. M. Response properties and receptive fields of cells in an anatomically defined region of the superior temporal sulcus in the monkey. *Brain Res.* 35: 528–532, 1971.
- FELLEMAN, D. J. AND VAN ESSEN, D. C. Cortical connections of area V3 in macaque extrastriate cortex. *Soc. Neurosci. Abstr.* 10: 933, 1984.
- FELLEMAN, D. J. AND VAN ESSEN, D. C. Receptive field properties of neurons in area V3 of macaque monkey extrastriate cortex. *J. Neurophysiol.* 57: 889–920, 1987.
- FELLEMAN, D. J. AND VAN ESSEN, D. C. Distributed hierarchical processing in the primate cerebral cortex. *Cereb. Cortex* 1: 1–47, 1991.
- FOSTER, K. H., GASKA, J. P., NAGLER, M., AND POLLEN, D. A. Spatial and temporal frequency selectivity of neurons in visual cortical areas V1 and V2 of the macaque monkey. *J. Physiol. Lond.* 365: 331–363, 1985.
- GALLYAS, F. Silver staining of myelin by means of physical development. *Neurol. Res.* 1: 203–209, 1979.
- GATTASS, R., SOUSA, A. P., AND GROSS, C. G. Visuotopic organization and extent of V3 and V4 of the macaque. *J. Neurosci.* 8: 1831–1845, 1988.
- GEGENFURTNER, K. R. AND HAWKEN, M. J. Temporal and chromatic properties of motion mechanisms. *Vision Res.* 35: 1547–1563, 1995.
- GEGENFURTNER, K. R., KIPER, D. C., BEUSMANS, J., CARANDINI, M., ZAIDI, Q., AND MOVSHON, J. A. Chromatic properties of neurons in macaque MT. *Visual Neurosci.* 11: 455–466, 1994.
- GEGENFURTNER, K. R., KIPER, D. C., AND FENSTEMAKER, S. B. Chromatic properties of neurons in macaque V2. *Soc. Neurosci. Abstr.* 19: 769, 1993.
- GEGENFURTNER, K. R., KIPER, D. C., AND FENSTEMAKER, S. B. Processing of color, form and motion in macaque area V2. *Visual Neurosci.* 13: 161–172, 1996.
- GIRARD, P., SALIN, P. A., AND BULLIER, J. Visual activity in areas V3A and V3 during reversible inactivation of area V1 in the macaque monkey. *J. Neurophysiol.* 66: 1493–1503, 1991.
- GREEN, D. G. The contrast sensitivity of the colour mechanisms of the human eye. *J. Physiol. Lond.* 196: 415–429, 1968.
- HAWKEN, M. J., PARKER, A. J., AND LUND, J. S. Laminar organization and contrast sensitivity of direction-selective cells in the striate cortex of the old world monkey. *J. Neurosci.* 8: 3541–3548, 1988.
- HAWKEN, M. J., SHAPLEY, R. M., AND GROSOF, D. H. Temporal frequency selectivity in monkey visual cortex. *Visual Neurosci.* 13: 477–492, 1996.
- HAYS, W. L. *Statistics* (3rd ed.). New York: CBS College, 1981.
- HESS, R. H., BAKER, C. L., JR., AND ZIHL, J. The “motion-blind” patient: low level spatial and temporal filters. *J. Neurosci.* 9: 1628–1640, 1989.
- JAMESON, D. AND HURVICH, L. M. Some quantitative aspects of an opponent colors theory. II. Brightness, saturation, and hue in normal and dichromatic vision. *J. Opt. Soc. Am.* 45: 602–616, 1955.
- KAPLAN, E. AND SHAPLEY, R. M. The primate retina contains two types of

- ganglion cells, with high and low contrast sensitivity. *Proc. Natl. Acad. Sci. USA* 83: 2755–2757, 1986.
- KELLY, D. H. Spatio-temporal frequency characteristics of color-vision mechanisms. *J. Opt. Soc. Am.* 64: 983–990, 1974.
- KRAUSKOPF, J., WILLIAMS, D. R., AND HEELEY, D. W. Cardinal directions of color space. *Vision Res.* 22: 1123–1131, 1982.
- LENNIE, P., KRAUSKOPF, J., AND SCLAR, G. Chromatic mechanisms in striate cortex of macaque. *J. Neurosci.* 10: 649–669, 1990.
- LEVITT, J. B., KIPER, D. C., AND MOVSHON, J. A. Receptive fields and functional architecture of macaque V2. *J. Neurophysiol.* 71: 2517–2542, 1994a.
- LEVITT, J. B., YOSHIOKA, T., AND LUND, J. S. Intrinsic cortical connections in macaque area V2: evidence for interaction between different functional streams. *J. Comp. Neurol.* 342: 551–570, 1994b.
- LIVINGSTONE, M. AND HUBEL, D. Segregation of form, color, movement and depth: anatomy, physiology and perception. *Science Wash. DC* 240: 740–750, 1988.
- LUND, J. Organisation of neurons in the visual cortex, area 17, of the monkey (*Macaca mulatta*). *J. Comp. Neurol.* 147: 455–495, 1973.
- MERIGAN, W. H., BYRNE, C. E., AND MAUNSELL, J. H. R. Does primate motion perception depend on the magnocellular pathway? *J. Neurosci.* 11: 3422–3429, 1991.
- MERRILL, E. G. AND AINSWORTH, A. Glass-coated platinum-plated tungsten microelectrode. *Med. Biol. Eng.* 10: 495–504, 1972.
- METHA, A. B., VINGRYS, A. J., AND BADCOCK, D. R. Detection and discrimination of moving stimuli: the effects of color, luminance, and eccentricity. *J. Opt. Soc. Am.* 11: 1697–1709, 1994.
- MOVSHON, J. A., ADELSON, E. H., GIZZI, M. S., AND NEWSOME, W. T. The analysis of moving visual patterns. In: *Pattern Recognition Mechanisms: Pontificiae Academiae Scientiarum Scripta Varia*, edited by C. Chagas, R. Gattass, and C. Gross. Rome: Vatican Press, 1985, vol. 54, p. 117–151.
- MOVSHON, J. A. AND NEWSOME, W. T. Visual response properties of striate cortical neurons projecting to area MT in macaque monkeys. *J. Neurosci.* 16: 7733–7741, 1996.
- O'KEEFE, L. P., CARANDINI, M., BEUSMANS, J. M. H., AND MOVSHON, J. A. MT neuronal responses to 1st- and 2nd-order motion. *Soc. Neurosci. Abstr.* 19: 1283, 1993.
- PETERHANS, E. AND VON DER HEYDT, R. Functional organization of area V2 in the alert macaque. *Eur. J. Neurosci.* 5: 509–524, 1993.
- SAITO, H., TANAKA, K., ISONO, H., YASUDA, M., AND MIKAMI, A. Directionally selective response of cells in the middle temporal area (MT) of the macaque monkey to movement of equiluminous opponent color stimuli. *Exp. Brain Res.* 75: 1–14, 1989.
- SAWATARI, A. AND CALLAWAY, E. M. Convergence of magno- and parvocellular pathways in layer 4B of macaque primary visual cortex. *Nature Lond.* 380: 442–446, 1996.
- SCHEIN, S. J. AND DESIMONE, R. Spectral properties of V4 neurons in macaque. *J. Neurosci.* 10: 3369–3389, 1990.
- SCLAR, G., MAUNSELL, J. H. R., AND LENNIE, P. Coding of image contrast in central visual pathways of the macaque monkey. *Vision Res.* 30: 1–10, 1990.
- SHADLEN, M. N., NEWSOME, W. T., ZOHARY, E., AND BRITTON, K. H. Integration of local motion signals in area MT. *Soc. Neurosci. Abstr.* 19: 1282, 1993.
- SHIPP, S., DE JONG, B. M., ZIHL, J., FRACKOWIAK, R. S. J., AND ZEKI, S. The brain activity related to residual motion vision in a patient with bilateral lesions of V5. *Brain* 117: 1023–1038, 1994.
- SHIPP, S. AND ZEKI, S. The organization of connections between areas V5 and V1 in macaque monkey visual cortex. *Eur. J. Neurosci.* 1: 309–322, 1989.
- STOCKMAN, A., MACLEOD, D. I., AND DEPRIEST, D. D. The temporal properties of the human short-wave photoreceptors and their associated pathways. *Vision Res.* 31: 189–208, 1991.
- STOCKMAN, A., MACLEOD, D. I., AND LEBRUN, S. J. Faster than the eye can see: blue cones respond to rapid flicker. *J. Opt. Soc. Am.* 10: 1396–1402, 1993.
- STROMEYER, C. F., III, KRONAUER, R. E., RYU, A., CHAPARRO, A., AND ESKEW, R. T. Contributions of human long-wave and middle-wave cones to motion detection. *J. Physiol. Lond.* 485.1: 221–243, 1995.
- UNGERLEIDER, L. G. AND MISHKIN, M. Two cortical visual systems. In: *Analysis of Visual Behavior*, edited by D. J. Ingle, M. A. Goodale, and R. J. W. Mansfield. Cambridge, MA: MIT Press, 1982, p. 549–586.
- VAN ESSEN, D. C., NEWSOME, W. T., MAUNSELL, J. H., AND BIXBY, J. L. The projections from striate cortex (V1) to areas V2 and V3 in the macaque monkey: asymmetries, areal boundaries, and patchy connections. *J. Comp. Neurol.* 244: 451–480, 1986.
- VAN ESSEN, D. C. AND ZEKI, S. M. The topographic organization of rhesus monkey prestriate cortex. *J. Physiol. Lond.* 277: 193–226, 1978.
- WILSON, H. R. AND KIM, J. A model for motion coherence and transparency. *Visual Neurosci.* 11: 1205–1220, 1994.
- WYSZECKI, G. AND STILES, W. S. *Color Science* (2nd ed.). New York: Wiley, 1982.
- ZEKI, S. M. Representation of central visual fields in prestriate cortex of monkey. *Brain Res.* 14: 271–291, 1969.
- ZEKI, S. M. The cortical projections of foveal striate cortex in the rhesus monkey. *J. Physiol. Lond.* 277: 227–244, 1978a.
- ZEKI, S. M. The third visual complex of rhesus monkey prestriate cortex. *J. Physiol. Lond.* 277: 245–272, 1978b.
- ZEKI, S. M. Uniformity and diversity of structure and function in rhesus monkey prestriate visual cortex. *J. Physiol. Lond.* 277: 273–290, 1978c.
- ZEKI, S. M. *A Vision of the Brain*. Oxford, UK: Blackwell, 1993.
- ZIHL, J., VON CRAMON, D., AND MAI, N. Selective disturbance of movement vision after bilateral brain damage. *Brain* 106: 313–340, 1983.